Binding mode and physiological role of epilepsy-related ligand/receptor LGI1-ADAM22 complex based on structural analysis

宮﨑　裕理

博士（理学）

総合研究大学院大学
生命科学研究科
生理科学専攻

平成３０（２０１８）年度

Binding mode and physiological role of epilepsy-related ligand/receptor LGI1-ADAM22 complex based on structural analysis

Miyazaki, Yuri

Doctor of Philosophy

SOKENDAI (The Graduate University for Advanced Studies)
School of Life Science
Department of Physiological Sciences

and

National Institute for Physiological Sciences
Department of Molecular and Cellular Physiology
Division of Membrane Physiology

2018

Acknowledgements

I gratefully acknowledge my research advisers Dr. Masaki Fukata and Dr. Yuko Fukata for all their support and advice for my PhD study. I thank the members of Fukata laboratory, Dr. Norihiko Yokoi, Dr. Tetsuya Hirata, Dr. Yoko Hirano, Mr. Hiroki Inahashi, Ms. Yumi Suzuki, Ms. Mie Watanabe and Ms. Sachiko Furukawa for kind supports.

I appreciate cooperation with many scientists, Dr. Shuya Fukai, Dr. Atsushi Yamagata, Dr. Yusuke Sato, Dr. Sakurako Goto-Ito and Ms. Asami Maeda (The University of Tokyo, Japan) for collaborating on the structural analysis of the LGI1–ADAM22 complex, Dr. Hideki Shigematsu and Dr. Mikako Shirouzu (RIKEN Center, Japan) for the Cryo-EM analysis of the LGI1–ADAM22 complex, Dr. Masumi Hirabayashi, Dr. Teppei Goto and Mr. Makoto Sanbo (National Institute for Physiological Sciences [NIPS], Japan) for generating transgenic mice.

I thank Dr. Toshitaka Kawarai (Tokushima University Graduate School, Japan) and Dr. Koji Sagane (Eisai Company, Japan) for providing the cDNAs of human *ADAM22* and *ADAM23*, respectively, and Dr. Masahiko Watanabe (Hokkaido University) for providing the guinea pig polyclonal antibody to LGI1.

I would like to thank my dissertation committee members, Dr. Yoshihiro Kubo, Dr. Kazuyoshi Murata (NIPS, Japan) and Dr. Katsuhiko Tabuchi (Shinshu University, Japan), for spending their precious time on my dissertation and for their constructive comments.

Lastly, I also thank my family for always supporting and encouraging me.

Table of Contents

Abbreviations

ADAM	A disintegrin and metalloprotease domain
ADLTE	Autosomal dominant lateral temporal lobe epilepsy
AMPA	α-amino-3-hydroxy-5-methyl-4-isoxazolepropionic acid
BSA	Bovine serum albumin
cDNA	Complementary DNA
Cryo-EM	Cryo-electron microscopy
DG	Dentate gyrus
DI	Disintegrin
DMEM	Dulbecco's modified Eagle's minimal essential medium
ECD	Ectodomain
EDTA	Ethylenediamine tetraacetate
EGF	Epidermal growth factor
EPTP	Epitempin
ER	Endoplasmic reticulum
GABA	γ-aminobutyric acid
HEK293	Human embryonic kidney 293
ID	Intellectual disability
IgG	Immunoglobulin G
IP	Immunoprecipitation
LE	Limbic encephalitis
LGI1	Leucine-rich glioma inactivated 1

LRR	Leucine-rich repeat
NMDA	N-methyl-d-aspartate
PBS	Phosphate buffered saline
PCR	Polymerase chain reaction
PDB	Protein data bank
PMSF	Phenylmethylsulfonyl fluoride
PSD-95	Postsynaptic density protein 95
TAP	Tandem-affinity purification
TARP	Transmembrane AMPA receptor regulatory protein
WT	Wild-type

Introduction

Epilepsy is one of the most common neurological disorders, which affects around 1% of the population. Epilepsy is featured by recurrent, unprovoked seizures, which are caused by imbalance between excitation and inhibition in neural circuits. Epilepsy-related mutations often occur in genes of ion channels regulating neuronal excitability, such as voltage-gated ion channels (K^+, Na^+ and Ca^{2+}) and ligand-gated ion channels (nicotinic acetylcholine and $GABA_A$ receptors)[1–3]. Some other epilepsy-related mutations have been found in genes encoding non-ion channel proteins such as Leucine-rich glioma inactivated 1 (*LGI1*).

LGI1 is a 60-kDa secreted neuronal protein, which consists of the N-terminal leucine-rich repeat (LRR) domain and the C-terminal epitempin-repeat (EPTP) (also known as EAR) domain[4]. Mutations of *LGI1* cause autosomal dominant lateral temporal lobe epilepsy (ADLTE; also known as autosomal dominant partial epilepsy with auditory features [ADPEAF])[5–7]. To date, at least 42 *LGI1* mutations have been reported in ADLTE families, including 28 missense mutations that are distributed in both the LRR and EPTP domains[5,6,8]. Most of the ADLTE missense mutations are secretion-defective[9], suggesting that they affect folding and/or posttranslational modifications of LGI1. Actually, secretion-defective $LGI1^{E383A}$ is recognized by the ER quality control machinery and prematurely degraded to cause epilepsy in a mouse model of ADLTE[9]. In addition to *LGI1* mutations in inherited epilepsy, autoantibodies against LGI1 most frequently occur with limbic encephalitis (LE) presenting with acquired amnesia and seizures in adult[10–12].

A disintegrin and metalloprotease 22 (ADAM22) is a member of transmembrane ADAM metalloproteases but is catalytically inactive. ADAM22 serves as a receptor for LGI1 and is anchored to the excitatory postsynaptic density through PSD-95 scaffold[13]. The LGI1–ADAM22 ligand-receptor interaction plays an essential role in AMPA-type glutamate receptor-mediated synaptic transmission *via* PSD-95[13–15]. A global LGI1 protein complex determined by proteomic analysis contains ADAM22 subfamily members (ADAM22, ADAM23 and ADAM11) as LGI1 receptors, postsynaptic scaffold proteins (PSD-95, PSD-93 and SAP97) and also presynaptic potassium channels (Kv1) and scaffolds (CASK and Lin7)[14,16]. Genetic evidence that loss of *Lgi1*[14,17,18], *Adam22*[19], *Adam23*[20,21] or *Kv1* channels[22,23] in mice causes a similar lethal epileptic phenotype supports their actions in a linear molecular pathway. Importantly, reported *LGI1* mutations[9], *ADAM22* mutations in a patient with seizures and intellectual disability[24], and LGI1 autoantibodies in patients with LE[12] all converge on the disruption of the LGI1–ADAM22 ligand-receptor interaction. Thus, LGI1–ADAM22 interaction is essential for physiological brain excitability and functions. LGI1 might serve as the ligand that tethers ADAM22 and ADAM23 at the synaptic cleft and *trans*-synaptically couple postsynaptic AMPA receptors on the PSD-95 platform with presynaptic machinery containing potassium channels[14,16].

In this study, I determined the mode of interaction of LGI1–ADAM22, based on the crystal structure determined by Dr. Fukai's group. Together with the structure-guided functional studies, I also revealed structural basis for pathogenesis of epilepsy that is associated with the *trans*-synaptic interaction mediated by the higher-order assembly of LGI1–ADAM22 subfamily

proteins.

Materials and Methods

All of the animal studies were reviewed and approved by the Institutional Animal Care and Use Committee of National Institutes of Natural Sciences and were performed in accordance with its guidelines concerning the care and handling of experimental animals.

Antibodies

The following commercially available antibodies were used: rabbit polyclonal antibodies to LGI1 (Abcam, ab30868, 1:100 for Western blotting) and ADAM23 (Abcam, ab28302, 1:200); mouse monoclonal antibodies to ADAM22 (NeuroMab, 75-083, 1:250 and 10 μg for immunoprecipitation), FLAG (Sigma-Aldrich, F3165, 1:1000) and β-catenin (BD Biosciences, 610153, 1:500). In addition, the following homemade antibodies were used: rabbit polyclonal antibodies to ADAM22 and ADAM23 were raised against GST-ADAM22 (mouse, residues 858–898, 1:1000) and GST-ADAM23 (mouse, residues 815–829, 10 μg for immunoprecipitation), respectively[9,14]. These antibodies were affinity purified on a CNBr-activated Sepharose 4B (GE Healthcare) column containing an immunizing antigen. A guinea pig polyclonal antibody to LGI1 (rat, residues 193–233, 1:500) was kindly provided by Dr. Masahiko Watanabe (Hokkaido University)[9].

Cloning and plasmid constructions

The cDNA of human *LGI1* (NM_005097) was purchased from Thermo Scientific (clone ID: 4811956). The cDNA of human *ADAM22* (same sequence as in NM_021723 except for the c.242C>G, p.Pro81Arg polymorphism in the Pro domain) was kindly provided by Dr. Toshitaka

Kawarai (Tokushima University Graduate School). The cDNA of human *ADAM23* (AB009672) was obtained from Dr. Koji Sagane (Eisai Company)[25]. For pull-down assays, the cDNA of human *LGI1* with or without His_6 tag at the 3' end together with 3'UTR and the cDNAs encoding the ectodomain (ECD) of human *ADAM22* (residues 35–729) and *ADAM23* (residues 61–790) with a FLAG tag at the 3' end were subcloned into cytomegalovirus promoter-driven expression vectors. To obtain ADAM22 ECD-FLAG and ADAM23 ECD-FLAG as soluble forms, Igκ signal peptide was used instead of authentic signal peptide sequences. For Fig. 5, the cDNAs encoding human $LGI1^{WT}$, $LGI1^{E123K}$ and $LGI1^{R474Q}$ (residues 37–557) tagged with His_6 were subcloned into pEBMulti-Neo with Igκ signal peptide. Indicated mutations were introduced by site-directed mutagenesis. All PCR products were analyzed by DNA sequencing (Functional Genomics Facility, NIBB or Fasmac Co., Ltd.). All primer sequences used in this study are shown in Table 1.

Cell culture and transfection

HEK293T cells were grown in Dulbecco's Modified Eagle Medium (DMEM, Sigma-Aldrich) supplemented with 10% fetal bovine serum (FBS, Sigma-Aldrich) at 37°C with 5% CO_2. After 14-20 h, HEK293T cells cells were transfected with plasmid DNAs by Lipofectamine and plus reagent system (Life technologies).

Pull-down assay

HEK293T cells were seeded onto 6-well plates ($3x10^5$ cells/well). Expression vectors for ADAM22 ECD-FLAG, ADAM23 ECD-FLAG, LGI1 and LGI1-His_6 (see 'Cloning and

plasmid constructions') were transfected into HEK293T cells, which were confirmed as mycoplasma-free. At 24 h after transfection, cells were washed with serum-free DMEM and cultured for an additional 24 h under serum-free conditions. Each conditioned medium was collected and mixed for 1 h at 4°C. LGI1-His_6 and ADAM22/23 ECD-FLAG were then purified by Ni-NTA agarose (Qiagen) and anti-FLAG M2 agarose (Sigma-Aldrich), respectively. The purified proteins were separated by SDS-PAGE and subjected to Western blotting with anti-FLAG and anti-LGI1 antibodies. For quantitative Western blotting, chemical luminescent signal was detected with a cooled CCD camera (Light-Capture II; ATTO) or the FUSION Solo system (Vilber-Lourmat). The band intensities were analyzed with CS analyzer 3.0 software (ATTO) or the FUSION Solo system.

Generation of transgenic mice

Lgi1 knockout mouse strain was previously established[14]. Briefly, embryonic stem cell clones with the targeted *Lgi1* locus were injected into C57BL/6 blastocysts. The chimeras were crossed with C57BL/6 mice for germ line transmission. Tandemly tagged $Lgi1^{R407C}$ and $Lgi1^{R474Q}$ transgenic mice (with FLAG and His_6 tags) were generated by DNA injection into fertilized embryos as for tandemly tagged $Lgi1^{WT}$ transgenic mice[14]. The injection was performed by Dr. Hirabayashi's group (NIPS). Briefly, the cDNA of $Lgi1^{R407C}$ or $Lgi1^{R474Q}$ with FLAG and His_6 tags was subcloned downstream of the Thy1 promoter[26]. Obtained transgenic founders were crossed with C57BL/6 mice and genotyping was performed using PCR primers shown in Table 1. For the rescue experiment, the $Lgi1^{+/-}$ mouse was crossbred with the individual transgenic strains. Obtained $Lgi1^{+/-;WT}$, $Lgi1^{+/-;R407C}$ or $Lgi1^{+/-;R474Q}$ was crossed with $Lgi1^{+/-}$ to obtain

Lgi1$^{-/-;WT}$, *Lgi1*$^{-/-;R407C}$ or *Lgi1*$^{-/-;R474Q}$ (referred to as *Lgi1*^{WT}, *Lgi1*^{R407C} or *Lgi1*^{R474Q}). Slightly prolonged lifetime of *Lgi1*^{R474Q} mice as compared with *Lgi1* null mice (Fig. 6A) is probably due to the still remaining functional tripartite complexes (Fig. 6E-H).

Subcellular fractionation

Brains from C57BL/6 mice were homogenized with 20 mM Tris-HCl (pH 8.0) buffer containing 2 mM EDTA, 320 mM sucrose and 200 μg mL^{-1} phenylmethylsulfonyl fluoride (PMSF). The homogenate was spun at 20,000 g for 1 h and supernatant was collected as S2 fraction. The pellet (crude synaptosomal fraction, P2 fraction) was solubilized with 20 mM Tris-HCl (pH 8.0) buffer containing 1.3% Triton X-100, 2 mM EDTA and 50 μg mL^{-1} PMSF. After centrifugation at 100,000 g for 1 h, the supernatant was collected as P2 soluble fraction (P2-sol) and pellets were re-homogenized with the same solubilization buffer to produce P2 insoluble fraction (P2-insol).

Tandem-affinity purification

Brains from *Lgi1*$^{-/-;WT}$ and *Lgi1*$^{-/-;R474Q}$ mice or from *Lgi1*$^{+/-;WT}$ and *Lgi1*$^{+/-;R407C}$ mice were homogenized and expressed LGI1^{WT}, LGI1^{R407C} or LGI1^{R474Q}-FLAG-His$_6$ was purified. Briefly, the P2-sol fraction from each mouse brain was prepared as described in 'Subcellular fractionation'. Each P2-sol fraction was incubated with anti-FLAG M2 agarose (SIGMA-aldrich) for 1 h at 4°C. The first eluate was obtained with 20 mM Tris-HCl (pH 7.5) buffer containing 100 mM NaCl, 1% Triton X-100, 50 μg mL^{-1} PMSF, 20 mM imidazole and 0.25 g L^{-1} FLAG peptide. The eluate was incubated with Ni-NTA agarose for 1 h at 4°C and the second

eluate was obtained with 20 mM Tris-HCl (pH 7.5) buffer containing 100 mM NaCl, 1% Triton X-100, 50 μg mL^{-1} PMSF and 250 mM imidazole. The purified proteins were separated by SDS-PAGE, subjected to silver staining or Western blotting.

Immunoprecipitation

For immunoprecipitation of ADAM22 or ADAM23 from mouse brain extracts (for Fig 6E-H, the indicated mouse strains; for Fig 9B, C57BL/6 mouse), The P2-sol fraction from each mouse brain was prepared as described in 'Subcellular fractionation'. Each P2-sol fraction was precleared with Protein A-Sepharose (GE Healthcare) and incubated with 10 μg of anti-ADAM22 or anti-ADAM23 antibody for 1h at 4°C. The immunecomplex was then precipitated with Protein A-Sepharose and eluted with SDS-PAGE sample buffer. Eluates were separated by SDS-PAGE and subjected to Western blotting.

Homology-model building and sequence alignments

For the prediction of three dimensional structural models of human ADAM23 (NP_003803), the homology modeling was performed by SWISS-MODEL server (https://swissmodel.expasy.org/) using the ADAM22 or LGI1 structure in LGI1–ADAM22 complex (PDB 5Y31 [http://dx.doi.org/10.2210/pdb5Y31/pdb])[27] determined by Dr. Fukai's group (The University of Tokyo) as a template. The putative interfaces of LGI family proteins–ADAM proteins were predicted by superposing the modeled structures onto the LGI1 EPTP–ADAM22 ECD interface (PDB 5Y2Z [http://dx.doi.org/10.2210/pdb5Y2Z/pdb])[27] determined by Dr. Fukai's group. PyMOL software (Schrödinger) was employed for the three-dimensional

graphics representation. Sequence alignments were performed by ClustalW2 run by European Molecular Biology Laboratory (https://www.ebi.ac.uk/Tools/msa/clustalw2/)[28].

Statistical analysis

To perform statistical analysis, at least 3 independent experiments, tissue samples or mice were included in the analyses. No statistical method was used to determine sample size. No data was excluded. There was no randomization of mice or samples before analysis, and the mice used in this study were selected based purely on availability. To appropriately choose and justify the statistical tests, I analyzed the normality of the data sets using skewness and kurtosis based on the normal probability plot and the variances between groups using F tests. If a data set was considered normal and the variance was similar between groups, then for paired sample comparisons, a two-tailed Student's t-test was used, and for multiple test subjects, one-way ANOVA with appropriate post hoc tests (as indicated in the figure legends) was used. If normal distribution was not observed or the variance was unequal, then to compare multiple groups against a control group, a nonparametric Kruskal-Wallis test followed by post hoc Steel's test was used; and to compare two independent groups, a Mann-Whitney U-test was used. Statistical analysis was performed with Ekuseru-Toukei 2012 software (SSRI). Results are shown as mean ± standard error.

Results

The mode of interaction of the LGI1–ADAM22 complex and physiological role of the complex formation

1. Structural features of LGI1–ADAM22 complex

LGI1 consists of the two domains, LRR and EPTP, and the mature ADAM22 consists of the extracellular four domains, transmembrane domain and cytoplasmic domain (**Figure 1A**). The C-terminal EPTP domain of LGI1 is sufficient for binding to the ectodomain (ECD) of ADAM22[13]. To investigate the mode of interaction between LGI1 and ADAM22, I focused on the X-ray crystal structure of the complex of LGI1 EPTP and ADAM22 ECD and that of the full-length LGI1 and ADAM22 ECD determined by Dr. Fukai's group (The University of Tokyo) (**Figure 1B, C**)[27]. In the crystal structure, the EPTP domain of LGI1 interacts with the metalloprotease-like domain of ADAM22 (**Figure 1B**). The full-length LGI1–ADAM22 ECD complex structure forms a 2:2 heterotetramer in the asymmetric unit of the crystal (**Figure 1C**). Two copies of the 1:1 LGI1–ADAM22 ECD complex are aligned in a head-to-head configuration with ~90° rotation along the longest axis. Besides the LGI1 EPTP–ADAM22 interactions, the LRR domain of one LGI1 molecule interacts with the EPTP domain of the other LGI1 molecule, thereby bridging two distant ADAM22 molecules in the complex (**Figure 1C**). The C-terminals of the two ADAM22 molecules are oriented in the opposite directions (**Figure 1C**).

2. Binding modes between LGI1 and ADAM22 or ADAM23

In the crystal structure, I found both hydrophobic and hydrogen-bonding interactions at the

interface between LGI1 and ADAM22. Trp398, Tyr408, and Tyr409 of ADAM22 are stacked in layer and project into the inner rim of the central channel of LGI1 EPTP to interact hydrophobically with Phe256, Val284, Leu302, Tyr433 and Met477 of LGI1 (**Figure 2A**). In addition, four hydrogen bonds are formed between LGI1 and ADAM22: Arg330 and Lys331 of LGI1 hydrogen bond with the side and main chains of Asp405 of ADAM22, respectively, and Lys353 and Arg378 of LGI1 hydrogen bond with Glu359 of ADAM22 (**Figure 2A**). To determine the critical residues for the interactions between LGI1 and ADAM22, I first mutated ADAM22-interacting residues of LGI1 into alanine and performed the pull-down assay with ADAM22 ECD (**Figure 2B** left, **C**). ADAM23, another LGI1 receptor, likely interacts with LGI1 in a manner similar to ADAM22, since the amino-acid sequence identity between ADAM22 and ADAM23 is substantially high (*e.g.*, ~50% between human ADAM22 and ADAM23). To compare the binding properties of LGI1 mutants to ADAM22 and ADAM23, I also examined the binding of LGI1 mutants to ADAM23 (**Figure 2B** right, **C**). The Y433A and M477A mutations of LGI1, which disturb the hydrophobic interaction with Tyr408 of ADAM22, almost abolished the binding to both ADAM22 and ADAM23 **(Figure 2B, C**). Tyr408 of ADAM22 is replaced by Val in ADAM23 (**Figure 2D**), which may also hydrophobically interact with Tyr433 and Met477 of LGI1. The F256A, V284A and L302A mutations of LGI1, which disturb the hydrophobic interaction with Trp398 of ADAM22, drastically impaired the binding to both ADAM22 and ADAM23 (**Figure 2B, C**). Greater effects of the F256A and V284A mutations of LGI1 on the binding to ADAM23 than on the binding to ADAM22 seem to be related to the difference in their hydrophobic interactions with Tyr433 and Met477 of LGI1; the replacement of Tyr408 in ADAM22 by Val in ADAM23

(**Figure 2D**) may decrease the total affinity of ADAM23 to LGI1. The R330A and K331A mutations of LGI1, which disable the hydrogen bonding with Asp405 of ADAM22, modestly impaired the binding to both ADAM22 and ADAM23 (**Figure 2B, C**). The R330A K331A double mutation almost abolished the binding (**Figure 2B, C**). Similarly, the K353A and R378A mutations of LGI1, which disable the hydrogen bonding with Glu359 of ADAM22, substantially impaired or almost abolished the binding to both ADAM22 and ADAM23 (**Figure 2B, C**). These results suggest that LGI1 binds to ADAM22 and ADAM23 in a similar manner.

I next mutated LGI1-interacting residues of ADAM22 and performed the pull-down assay with LGI1 (**Figure 3A, B**). The W398D, Y408A, Y409A or Y408A Y409A mutation of ADAM22 almost or completely abolished its binding to LGI1, indicating that the hydrophobic interaction mediated by Trp398, Tyr408 and Tyr409 of ADAM22 is essential for binding between LGI1 and ADAM22 (**Figure 3A, B**). On the other hand, the E359A or D405A mutation of ADAM22 decreased but did not abolish its binding to LGI1. The hydrogen bonds play a secondary role in binding between LGI1 and ADAM22 (**Figure 3A, B**). To ask whether the essential hydrophobic interaction in the LGI1–ADAM22 interface is conserved in the LGI1–ADAM23 interface, I mutated Trp455, Val466 and Ser467 of ADAM23 corresponding to Trp398, Tyr408 and Tyr409 of ADAM22, and examined their binding to LGI1 (**Figure 3C, D**). Consistently, the W456D and V466A mutations of ADAM23 robustly decreased its binding to LGI1. In contrast, the S467A mutation of ADAM23 did not affect its binding to LGI1, indicating that Ser467 is not incorporated into the hydrophobic interaction. These results indicate that the essential hydrophobic interactions are basically conserved in the interfaces of LGI1–ADAM22

and LGI1–ADAM23 (**Figure 3E**) and that a single LGI1 molecule cannot bind simultaneously to both ADAM22 and ADAM23. Given that Tyr409 of ADAM22, but not the corresponding Ser467 of ADAM23, is essential for the LGI1 binding, it is conceivable that ADAM22 has a higher binding affinity to LGI1 than ADAM23.

3. Structural insights into epilepsy-related mutations in *LGI1* and *ADAM22*

To date, at least 42 *LGI1* mutations have been reported in patients with familial ADLTE[9,29–32]. To gain structural insights into pathogenic mechanisms of these mutations, I mapped 28 missense mutations (**Figure 4A**) onto the determined LGI1 structure (**Figure 4B and Table 2**). Nineteen of the examined missense mutations are secretion-defective (shown in red color), likely owing to failure of protein folding[9,33]. Correspondingly, the C42R, C42G, C46R, C46F, C179R and C200R mutations disrupt intramolecular disulfide bonds in the N- and C-terminal caps of LGI1 LRR (**Figure 4B**), which are common in extracellular and membrane-associated LRR proteins to stabilize their N- and C-terminal edges[34]. The E383A mutation disables the water-mediated Ca^{2+} coordination by the side chains of Asp334, Glu336 and Asp381, the main-chain O atom of Val382 and a water molecule bound to Glu383 that stabilizes the β-propeller structure of LGI1 EPTP (**Figure 4C**). Other secretion-defective mutations affect structural cores inside LGI1 LRR or EPTP (**Figure 4B**). To further ask if the amino-acid alterations which do not affect the structural stabilization are basically nonpathogenic, I took advantage of gnomAD database (the Genome Aggregation Database; http://gnomad.broadinstitute.org/). Because the data of individuals with severe diseases are basically excluded, I assumed that the numerous variants in the database may provide the useful information to predict the pathogenic

amino-acid alterations. I mapped 144 LGI1 variants with amino-acid alterations in the cording region except for the signal sequence) listed in the gnomAD database onto the determined LGI1 structure (**Figure 4D and Table 3**). Most of LGI1 variants listed in the gnomAD were mapped beyond the structural cores of LGI1 (**Figure 4D**). Although some of the amino-acid variants are located at the structural cores inside the domains (*e.g.,* I82L, S402C and I491V), these amino acids are replaced by those with the similar properties (*e.g.,* charge and hydrophobicity). Interestingly, one LGI1 variant, R330Q, occurs at the interface to ADAM22 (**Figure 2A**). However, a single alanine mutation of Arg330 did not robustly reduce the binding of ADAM22 in the pull-down assay (~20% reduction) (**Figure 2B, C**), suggesting that the R330Q substitution does not affect the function.

Three secretion-competent mutations, R407C, S473L and R474Q, are basically located at the protein surface of LGI1 EPTP[9,35–37] (**Figure 4A, B**; shown in blue color). The S473L mutation specifically impairs the binding to ADAM22 *in vivo*[9], although Ser473 is located distant from the ADAM22-intearcting region (**Figure 4B**). One possible mechanism for this ADAM22-specific impairment of the binding by the S473L mutation is that Phe451 of LGI1, which is located in the vicinity of Ser473 (<5 Å), may shift and cause a steric hindrance with Tyr408 and/or Lys362 of ADAM22 (**Figure 4E**). In the LGI1 EPTP–ADAM22 ECD structure, Phe451 of LGI1 is 5–6-Å apart from Tyr408 and/or Lys362 of ADAM22, which are replaced by amino-acid residues of shorter side chains in ADAM23 and ADAM11 (Val/Leu and Phe/Asn, respectively) to avoid steric hindrance with Phe451 of LGI1. Because Arg407 and Arg474 of LGI1 are not involved in the LGI1–ADAM22 interface, it is possible that the pathogenesis of

the R407C and R474Q mutations is related to other structural mechanisms (described below). The information on the ADLTE-associated mutations described here was summarized as **Table 2**.

In addition to *LGI1* mutations, the structure of LGI1–ADAM22 heterodimer provided an insight into pathogenic mechanism for a recently identified mutation in *ADAM22*[24]. The C401Y mutation of ADAM22 has been found in a patient with rapidly progressing severe encephalopathy with intractable seizures and profound intellectual disability[24]. Consistently, the C401Y mutation of ADAM22 impairs the binding to LGI1 *in vitro*[24]. The apo structure of ADAM22 ECD[38] (PDB 3G5C [http://dx.doi.org/10.2210/pdb3G5C/pdb]) is essentially the same as the LGI1-bound structure, except for the Trp398- and Tyr408–Tyr409-containing loops (**Figure 4F**). These aromatic residues are buried inside the protein in the apo state and become exposed to LGI1 EPTP upon binding. Mechanistically, Lys331 and Arg378 of LGI1 appear to eject the side chains of Tyr409 and Tyr408 of ADAM22, respectively. The disulfide bond between Cys394 and Cys401 tethers the N- and C-terminal ends of the Trp398-containing loop to support its conformational change (**Figure 4F**). Trp398, Cys394 and Cys401 are completely conserved in ADAM11, ADAM22 and ADAM23 (**Figure 2D**).

4. Defect in higher-order LGI1−ADAM22 assembly by the ADLTE mutation

It has been reported that LGI1 connects between ADAM22 and ADAM23 in the mouse brain and that the LGI1-associated protein complex contains both presynaptic and postsynaptic proteins[14]. In addition, the determined structure of LGI1–ADAM22 complex and the binding

modes between LGI1 and ADAM22 or ADAM23 suggests that 1) the length along the longest axis of the 2:2 LGI1–ADAM22 ECD complex is about 190 Å which is equivalent to the length of a synaptic cleft (**Figure 1C**) and 2) ADAM22 and ADAM23 do not simultaneously bind to a single LGI1 molecule (**Figure 3**). Taken together, I hypothesized that LGI1 *trans*-synaptically tethers two receptors, ADAM22 and ADAM23, through the intermolecular interaction between two LGI1 molecules (LGI1–LGI1 interaction), observed in the crystal structure of the 2:2 LGI1–ADAM22 ECD complex (**Figure 1C**). Therefore, I focused on the 2:2 heterotetrameric assembly of LGI1–ADAM22.

In the 2:2 heterotetrameric structure of the LGI1–ADAM22 ECD complex, I found that the intermolecular interactions occur between LRR and EPTP and between LRR and ADAM22 ECD (**Figure 5A**): Glu123 and Arg76 in the LRR domain of one LGI1 likely form hydrogen bonds with Arg474 and Glu516 in the EPTP domain of the other LGI1, respectively, to mediate the LGI1–LGI1 interaction. His116 of LGI1 LRR likely interacts with Glu446 in the disintegrin domain of ADAM22. It should be noted that two human ADLTE mutations, E123K[39] and R474Q[36], occur at the amino-acid pair possibly involved in the LGI1–LGI1 interaction (**Figure 5A**). Although the secretion of $LGI1^{E123K}$ ($LGI1^{E123K}$; superscripts attached with protein names hereafter denote their mutations) was heavily disturbed, $LGI1^{R474Q}$ protein was normally secreted from transfected HEK293T cells as $LGI1^{WT}$ (**Figure 5B**)[9]. It is strongly suggested that R474Q is pathogenic to impair the LGI1–LGI1 interaction, without affecting the folding of LGI1.

To assess the pathogenic mechanism of the R474Q mutation, I first examined the *in vitro* binding of LGI1^{R474Q} to ADAM22 or ADAM23 by the pull-down assay. LGI1^{R474Q} bound to ADAM22 and ADAM23 as LGI1^{WT} did (**Figure 5C**), indicating that the R474Q mutation is a very unique mutation which does not affect either the secretion nor the binding activity to the receptors, ADAM22 and ADAM23. Next, to investigate whether the R474Q mutation affects the higher-order LGI1–ADAM22 assembly, the molar mass of the LGI1–ADAM22 ECD complex was determined by size-exclusion chromatography coupled with multi-angle laser light scattering (SEC-MALS) (based on the collaboration with Dr. Fukai's group)[27]. The determined molar mass of LGI1^{WT}–ADAM22 ECD was 267 kDa, corresponding to the 2:2 heterotetrameric assembly of LGI1 and ADAM22 ECD, whereas that of LGI1^{R474Q}–ADAM22 ECD complex was 134 kDa, corresponding to the theoretical molar mass of the 1:1 complex of LGI1 and ADAM22 ECD (117 kDa; without sugar chains). These results indicate that the R474Q mutation of LGI1 prevents the higher-order assembly of LGI1–ADAM22 ECD, by disrupting the LGI1–LGI1 interaction between two LGI1–ADAM22 heteroassemblies.

5. Disruption of the synaptic linkage by a defect in LGI1–LGI1 interaction causes epilepsy

To prove the pathogenic mechanism of the R474Q mutation *in vivo*, I performed the transgenic rescue experiment with the *Lgi1* knockout mice. The transgenic mice were generated by Dr. Hirabayashi's group (NIPS). Homozygous null *Lgi1*$^{-/-}$ mice, which showed spontaneous recurrent generalized seizures and premature death, could be rescued by the reexpression of *Lgi1*^{WT} transgene (*Lgi1*$^{-/-;WT}$; superscripts attached with protein names hereafter denote their mutations)[14] (**Figure 6A**). In striking contrast, the reexpression of *Lgi1*^{R474Q} transgene (*Lgi1*$^{-}$

$^{/-;R474Q}$) could not rescue the epileptic phenotype of the *Lgi1*$^{-/-}$ mouse, showing the premature death due to the lethal epilepsy (**Figure 6A**). The expression level of LGI1^{R474Q} protein in the *Lgi1*$^{-/-;R474Q}$ mutant mouse was similar to that of LGI1^{WT} protein (**Figure 6B**). Given that the R474Q mutation of LGI1 is actually pathogenic to cause epilepsy in mice (**Figure 6A**), the structure of the 2:2 LGI1–ADAM22 complex supports the notion that the pathogenic mechanism of LGI1^{R474Q} is a defect in the assembly of the heterotetrameric ADAM22–LGI1–LGI1–ADAM22/23 complex in synapses.

I next tandem-affinity purified the LGI1 protein complexes from mouse brains in which LGI1^{WT} or LGI1^{R474Q} tagged with FLAG and His_6 was reexpressed in the *Lgi1* knockout background. I obtained similar band patterns between LGI1^{WT}- and LGI1^{R474Q}-containing protein complexes, showing the interactions with ADAM22, ADAM23 and PSD-95 (**Figure 6C**). Quantitative Western blotting showed that the LGI1^{R474Q} binding to ADAM23 was intact, whereas its binding to ADAM22 was reduced as compared with the LGI1^{WT} binding (42.8 ± 0.6% reduction) (**Figure 6D**). However, the partially reduced LGI1^{R474Q} binding to ADAM22 is not sufficient to cause the lethality of *Lgi1*$^{-/-;R474Q}$ mutant mice, as ADAM22 heterozygous knockout mice do not show any epileptic phenotypes (with 50% of the LGI1–ADAM22 interaction)[19]. I then asked if the LGI1–LGI1 interaction is affected by the R474Q mutation in the brain. When ADAM23 was immunoprecipitated from brain extracts of the wild-type mouse brain, ADAM22 was co-immunoprecipitated completely in an LGI1-dependent manner, indicating that ADAM22 and ADAM23 occur in a tripartite protein complex together with LGI1 (**Figure 6E**; *Lgi1*$^{+/+}$ versus *Lgi1*$^{-/-}$)[14]. The tripartite complex formation was restored by

the reexpression of LGI1^{WT} (*Lgi1*$^{-/-;WT}$). Importantly, the co-immunoprecipitation of ADAM22 with ADAM23 was robustly reduced in *Lgi1*$^{-/-;R474Q}$ mouse brain (79.9 ± 3.6% reduction) as compared with that in the *Lgi1*$^{-/-;WT}$ mouse brain (**Figure 6F**). Given that LGI1^{R474Q} has the intact binding ability to ADAM23 and partially reduced binding to ADAM22 (less than 50% reduction) (**Figure 6D**), the LGI1–LGI1 interaction is primarily reduced in the *Lgi1*$^{-/-;R474Q}$ mouse brain (estimated to be ~35% of that in the *Lgi1*$^{-/-;WT}$ mouse brain). Reciprocally, co-immunoprecipitation of ADAM23 with ADAM22 was heavily reduced in *Lgi1*$^{-/-;R474Q}$ mouse brain (**Figure 6G, H**). Thus, LGI1–ADAM22 and LGI1–ADAM23 are assembled into higher-order heteromers (at least, heterotetramers) *in vivo* and the disruption of the inter-LGI1 interactions causes epilepsy in an ADLTE mouse model (**Figure 6I**).

I also investigated the R407C mutation of LGI1, the other secretion-competent mutation. The R407C mutation of LGI1 did not affect the binding to ADAM22 *in vitro* (**Figure 7A**). The lethal epileptic phenotypes of *Lgi1* knockout mice could be rescued by reexpression of *Lgi1*^{R407C} transgene (*Lgi1*$^{-/-;R407C}$) in the brain (**Figure 6A**), in contrast to *Lgi1*$^{-/-;S473L}$ and *Lgi1*$^{-/-;R474Q}$ (**Figure 6A**)[9]. Furthermore, when the expressed LGI1^{R407C} was purified from the mouse brain, LGI1^{R407C} bound to ADAM22 and ADAM23 as LGI1^{WT} did **(Figure. 7B).** Consistently, LGI1^{R407C} variant was found in 5 gnomAD controls. I thus conclude that R407C is not a pathogenic mutation for ADLTE.

In conclusion, I propose that LGI1–ADAM22/ADAM23 functions as higher-order assembly for the *trans*-synaptic linkage and that its disruption causes abnormal brain excitability,

resulting in epilepsy in mice **(Figure. 8)**.

Discussion

In this study, I determined the mode of interaction of LGI1–ADAM22 complex and proposed that the LGI1–ADAM22 complex functions as the *trans*-synaptic machinery for precise synaptic transmission. However, one may ask whether the LGI1–ADAM22 complex actually links the presynapse and postsynapse.

Previous studies have supported that there are interdependent interactions between postsynaptic ADAM22 and presynaptic ADAM23 involving LGI1 at least in the molecular layer of the dentate gyrus (DG), representing tripartite *trans*-synaptic complexes[9]. Specifically, the *in vivo* LGI1-associated protein complex includes both postsynaptic (PSD-95, PSD-93 and SAP97) and presynaptic (CASK, Lin7 and Kv1) proteins[14]. Furthermore, ADAM23 protein in the outer/middle molecular layers of the DG is apparently reduced in ADAM22 and LGI1 knockout mice[9]. ADAM23 protein localized in the DG represents totally presynaptic one derived from the entorhinal cortex, because there is no expression of ADAM23 mRNA in dentate granule cells[12,21]. mRNAs of ADAM22 and LGI1 are highly expressed in dentate granule cells and the corresponding proteins are enriched in the dentate molecular layer[9,12]. In the structure of the 2:2 LGI1–ADAM22 complex, the C-terminals of the two ADAM22 ECD molecules are oriented in the opposite directions (**Figure 1C**) and the length along the longest axis is about 190 Å, which matches the height of the synaptic cleft. These two structural features support the idea that the heterotetrameric assembly of the LGI1–ADAM22 complex reflects the *trans*-synaptic linkage mediated by the tripartite complex of ADAM23–LGI1–ADAM22.

In addition to the 2:2 heterotetrameric assembly of LGI1–ADAM22, the size-exclusion chromatography coupled with multi-angle laser light scattering (SEC-MALS), small angle X-ray scattering (SAX) and cryo-electron microscopy (EM) analyses of the LGI1–ADAM22 ECD complex performed by Dr. Fukai's group (The University of Tokyo) and Dr. Shigematsu's group (RIKEN center) also suggested the presence of the 3:3 heterohexamer in solution[27]. Based on the mode of interactions, it seems feasible that three LGI1 molecules can bridge three ADAM22 molecules. In both assemblies, the important point is that LGI1 bridges two ADAM22 molecules with the LRR–EPTP interaction between the two adjacent LGI1 molecules and the disruption of inter-LGI1 interaction prevents both 2:2 and 3:3 assembly. In the 3:3 LGI1–ADAM22 assembly model, the C-terminals of two of the three ADAM22 ECD molecules are also oriented in the opposite directions and the length along the longest axis is about 160 Å. Nevertheless, I cannot exclude the possibility that a *cis*-interaction between LGI1 and ADAM22/ADAM23 on the same pre- or postsynaptic membrane occurs under some circumstances. The immunohistochemical studies will be required to precisely localize LGI1, ADAM22 and ADAM23 in the brain.

Given the essential roles of LGI1, ADAM22 and ADAM23 in epileptogenesis, LGI1–ADAM22 subfamily tetramers or hexamers may have unique and distinct functions from other numerous *trans*-synaptic cell adhesion molecules such as neurexin–neuroligin[40]. Recent super-resolution imaging revealed a *trans*-synaptic nanocolumn that aligns nanometer-scale synaptic subregions, presynaptic RIM-containing nanodomains and postsynaptic PSD-95-organizing nanodomains, for precise synaptic transmission[41]. Because ADAM22 directly binds to the third

PDZ domain of PSD-95[13], LGI1–ADAM22 subfamily tetramers may participate in the *trans*-synaptic nanocolumn formation through unknown presynaptic partners. Alternatively, LGI1–ADAM22 tetramers may stabilize the PSD-95 platform as an extracellular scaffold and thereby activate binding activities of PSD-95 at the first/second PDZ domains to AMPA receptor/TARP[42], NMDA receptor[43], and Kv1 channels[44]. Consistently, loss of LGI1 and ADAM22 reduces AMPA receptor currents[14] and Kv1 expression[14,45] . Future analysis will need to clarify the mode of action of LGI1–ADAM22–PSD-95 supramolecular complex and the molecular mechanisms of epileptogenesis.

Lastly, I propose that LGI family–ADAM22 subfamily represents an intriguing therapeutic target for epilepsy and other neurological disorders. I hope that my study will contribute to a better understanding of disease-causing mechanisms and facilitate the development of therapeutics for epilepsy and other neurological disorders by serving as a useful platform for structure-based design.

References

1. Steinlein, O. K. Genetic mechanisms that underlie epilepsy. *Nat. Rev. Neurosci.* **5,** 400–408 (2004).
2. Fukata, Y. & Fukata, M. Epilepsy and synaptic proteins. *Curr. Opin. Neurobiol.* **45,** 1–8 (2017).
3. Noebels, J. Pathway-driven discovery of epilepsy genes. *Nat. Neurosci.* **18,** 344–350 (2015).
4. Staub, E. *et al.* The novel EPTP repeat defines a superfamily of proteins implicated in epileptic disorders. *Trends Biochem. Sci.* **27,** 441–444 (2002).
5. Gu, W. *et al.* The LGI1 gene involved in lateral temporal lobe epilepsy belongs to a new subfamily of leucine-rich repeat proteins. *FEBS Lett.* **519,** 71–76 (2002).
6. Kalachikov, S. *et al.* Mutations in LGI1 cause autosomal-dominant partial epilepsy with auditory features. *Nat. Genet.* **30,** 335–41 (2002).
7. Morante-Redolat, J. M. *et al.* Mutations in the LGI1/Epitempin gene on 10q24 cause autosomal dominant lateral temporal epilepsy. *Hum. Mol. Genet.* **11,** 1119–1128 (2002).
8. Ottman, R. *et al.* LGI1 mutations in autosomal dominant partial epilepsy with auditory features. *Neurology* **62,** 1120–6 (2004).
9. Yokoi, N. *et al.* Chemical corrector treatment ameliorates increased seizure susceptibility in a mouse model of familial epilepsy. *Nat. Med.* **21,** 19–26 (2015).
10. Lai, M. *et al.* Investigation of LGI1 as the antigen in limbic encephalitis previously attributed to potassium channels: A case series. *Lancet Neurol.* **9,** 776–785 (2010).
11. Irani, S. R. *et al.* Antibodies to Kv1 potassium channel-complex proteins leucine-rich, glioma inactivated 1 protein and contactin-associated protein-2 in limbic encephalitis, Morvan's syndrome and acquired neuromyotonia. *Brain* **133,** 2734–2748 (2010).
12. Ohkawa, T. *et al.* Autoantibodies to epilepsy-related LGI1 in limbic encephalitis neutralize LGI1-ADAM22 interaction and reduce synaptic AMPA receptors. *J. Neurosci.* **33,** 18161–74 (2013).
13. Fukata Y, Adesnik H, Iwanaga T, Bredt DS, Nicoll RA, F. M. Epilepsy-Related Ligand/Receptor Complex LGI1 and ADAM22 Regulate Synaptic Transmission. *Science.* **313,** 1792–1795 (2006).
14. Fukata, Y. *et al.* Disruption of LGI1-linked synaptic complex causes abnormal synaptic transmission and epilepsy. *Proc. Natl. Acad. Sci. U. S. A.* **107,** 3799–804 (2010).

15. Lovero, K. L., Fukata, Y., Granger, A. J., Fukata, M. & Nicoll, R. A. The LGI1-ADAM22 protein complex directs synapse maturation through regulation of PSD-95 function. *Proc. Natl. Acad. Sci. U. S. A.* **112,** E4129-37 (2015).
16. Schulte, U. *et al.* The epilepsy-linked Lgi1 protein assembles into presynaptic Kv1 channels and inhibits inactivation by Kvβ1. *Neuron* **49,** 697–706 (2006).
17. Chabrol, E. *et al.* Electroclinical characterization of epileptic seizures in leucine-rich, glioma-inactivated 1-deficient mice. *Brain* **133,** 2749–2762 (2010).
18. Yu, Y. E. *et al.* Lgi1 null mutant mice exhibit myoclonic seizures and CA1 neuronal hyperexcitability. *Hum. Mol. Genet.* **19,** 1702–1711 (2010).
19. Sagane, K. *et al.* Ataxia and peripheral nerve hypomyelination in ADAM22-deficient mice. *BMC Neurosci* **6,** 33 (2005).
20. Mitchell, K. J. *et al.* Functional analysis of secreted and transmembrane proteins critical to mouse development. *Nat. Genet.* **28,** 241–249 (2001).
21. Owuor, K. *et al.* LGI1-associated epilepsy through altered ADAM23-dependent neuronal morphology. *Mol. Cell. Neurosci.* **42,** 448–457 (2009).
22. Brew, H. M. *et al.* Seizures and Reduced Life Span in Mice Lacking the Potassium Channel Subunit Kv1.2, but Hypoexcitability and Enlarged Kv1 Currents in Auditory Neurons. *J. Neurophysiol.* **98,** 1501–1525 (2007).
23. Smart, S. L. *et al.* Deletion of the K(v)1.1 Potassium channel causes epilepsy in mice. *Neuron* **20,** 809–819 (1998).
24. Muona, M. *et al.* Dysfunctional ADAM22 implicated in progressive encephalopathy with cortical atrophy and epilepsy. *Neurol. Genet.* **2,** e46 (2016).
25. Sagane, K., Ohya, Y., Hasegawa, Y. & Tanaka, I. Metalloproteinase-like, disintegrin-like, cysteine-rich proteins MDC2 and MDC3: novel human cellular disintegrins highly expressed in the brain. *Biochem. J.* **334 (Pt 1,** 93–8 (1998).
26. Lüthi, A. *et al.* Endogenous serine protease inhibitor modulates epileptic activity and hippocampal long-term potentiation. *J. Neurosci.* **17,** 4688–99 (1997).
27. Yamagata, A. *et al.* Structural basis of epilepsy-related ligand–receptor complex LGI1–ADAM22. *Nat. Commun.* **9,** 1546 (2018).
28. Larkin, M. A. *et al.* Clustal W and Clustal X version 2.0. *Bioinformatics* **23,** 2947–2948 (2007).
29. Nobile, C. *et al.* LGI1 mutations in autosomal dominant and sporadic lateral temporal epilepsy. *Hum. Mutat.* **30,** 530–536 (2009).

30. Lee, M. K. *et al.* A newly discovered LGI1 mutation in Korean family with autosomal dominant lateral temporal lobe epilepsy. *Seizure* **23,** 69–73 (2014).
31. Sadleir, L. G. *et al.* Seizure semiology in autosomal dominant epilepsy with auditory features, due to novel LGI1 mutations. *Epilepsy Res.* **107,** 311–317 (2013).
32. Dazzo, E. *et al.* Autosomal dominant lateral temporal epilepsy (ADLTE): Novel structural and single-nucleotide LGI1 mutations in families with predominant visual auras. *Epilepsy Res.* **110,** 132–138 (2015).
33. Leonardi, E. *et al.* A computational model of the LGI1 protein suggests a common binding site for ADAM proteins. *PLoS One* **6,** (2011).
34. Bella, J., Hindle, K. L., McEwan, P. A. & Lovell, S. C. The leucine-rich repeat structure. *Cell. Mol. Life Sci.* **65,** 2307–2333 (2008).
35. Striano, P. *et al.* Familial temporal lobe epilepsy with psychic auras associated with a novel LGI1 mutation. *Neurology* **76,** 1173–1176 (2011).
36. Kawamata, J. *et al.* Mutations in LGI1 gene in japanese families with autosomal dominant lateral temporal lobe epilepsy: the first report from asian families. *Epilepsia* **51,** 690–693 (2010).
37. Dazzo, E. *et al.* Secretion-Positive LGI1 Mutations Linked to Lateral Temporal Epilepsy Impair Binding to ADAM22 and ADAM23 Receptors. *PLoS Genet.* **12,** 1–15 (2016).
38. Liu, H., Shim, A. H. R. & He, X. Structural characterization of the ectodomain of a disintegrin and metalloproteinase-22 (ADAM22), a neural adhesion receptor instead of metalloproteinase. Insights on adam function. *J. Biol. Chem.* **284,** 29077–29085 (2009).
39. Bonaventura, C. Di *et al.* Drug resistant ADLTE and recurrent partial status epilepticus with dysphasic features in a family with a novel LGI1mutation: Electroclinical, genetic, and EEG/fMRI findings. *Epilepsia* **50,** 2481–2486 (2009).
40. Bemben, M. A., Shipman, S. L., Nicoll, R. A. & Roche, K. W. The cellular and molecular landscape of neuroligins. *Trends Neurosci.* **38,** 496–505 (2015).
41. Tang, A. H. *et al.* A trans-synaptic nanocolumn aligns neurotransmitter release to receptors. *Nature* **536,** 210–214 (2016).
42. Nicoll, R. A. Auxiliary Subunits Assist AMPA-Type Glutamate Receptors. *Science.* **311,** 1253–1256 (2006).
43. Niethammer, M., Kim, E. & Sheng, M. Interaction between the C terminus of NMDA

receptor subunits and multiple members of the PSD-95 family of membrane-associated guanylate kinases. *J. Neurosci.* **16,** 2157–63 (1996).

44. Becker, J. W. *et al.* Stromelysin-1: Three-dimensional structure of the inhibited catalytic domain and of the C-truncated proenzyme. *Protein Sci.* **4,** 1966–1976 (1995).
45. Seagar, M. *et al.* LGI1 tunes intrinsic excitability by regulating the density of axonal Kv1 channels. *Proc. Natl. Acad. Sci.* (2017).
46. Berkovic, S. F. *et al.* LGI1 mutations in temporal lobe epilepsies. *Neurology* **62,** 1115–1119 (2004).
47. Gu, W., Brodtkorb, E. & Steinlein, O. K. LGI1 is mutated in familial temporal lobe epilepsy characterized by aphasic seizures. *Ann. Neurol.* **52,** 364–367 (2002).
48. Pizzuti, A. *et al.* Epilepsy with auditory features: A LGI1 gene mutation suggests a loss-of-function mechanism. *Ann. Neurol.* **53,** 396–399 (2003).
49. Striano, P. *et al.* A novel loss-of-function LGi1 mutation linked to autosomal dominant lateral temporal epilepsy. *Arch. Neurol.* **65,** 939–942 (2008).
50. Di Bonaventura, C. *et al.* Low penetrance and effect on protein secretion of LGI1 mutations causing autosomal dominant lateral temporal epilepsy. *Epilepsia* **52,** 1258–1264 (2011).
51. Michelucci, R. *et al.* A de novo LGI1 mutation causing idiopathic partial epilepsy with telephone-induced seizures. *Neurology* **68,** 2150–2151 (2007).
52. Hedera, P. *et al.* Autosomal Dominant Lateral Temporal Epilepsy: Two Families with Novel Mutations in the LGI1 Gene. *Epilepsia* **45,** 218–222 (2004).
53. Pisano, T. *et al.* Abnormal phonologic processing in familial lateral temporal lobe epilepsy due to a new LGII mutation. *Epilepsia* **46,** 118–123 (2005).
54. Michelucci, R. *et al.* Autosomal Dominant Lateral Temporal Epilepsy: Clinical Spectrum, New Epitempin Mutations, and Genetic Heterogeneity in Seven European Families. *Epilepsia* **44,** 1289–1297 (2003).
55. Klein, K. M. *et al.* Autosomal dominant epilepsy with auditory features: a new LGI1 family including a phenocopy with cortical dysplasia. *J. Neurol.* **263,** 11–16 (2016).
56. Fumoto, N. *et al.* Novel *LGI1* mutation in a Japanese autosomal dominant lateral temporal lobe epilepsy family. *Neurol. Clin. Neurosci.* **5,** 44–45 (2017).
57. Chabrol, E. *et al.* Two novel epilepsy-linked mutations leading to a loss of function of LGI1. *Arch. Neurol.* **64,** 217–222 (2007).
58. Fertig, E., Lincoln, A., Martinuzzi, A., Mattson, R. H. & Hisama, F. M. Novel LGI1

mutation in a family with autosomal dominant partial epilepsy with auditory features. *Neurology* **60,** 1687–1690 (2003).

59. Heiman, G. A. *et al.* Evaluation of depression risk in LGI1 mutation carriers. *Epilepsia* **51,** 1685–1690 (2010).

Table 1. Summary of primers used in this study

Purpose	Primer Name	Primer Sequence (5' to 3')	Description
human LGI1 (1-557)-3'UTR expression	kozak hLGI1-EcoRI -F	GCTAGAATTCGACTGCATGGAATCAGA AAGAAGCAAAAG	Forward primer to subclone human LGI1 sequence with 3'UTR into pEGFP-N2 vector
	hLGI1 3'UTR-EcoRI -R	GCTAGAATTCTTTATGAAAGAAAATGTA AACAT	Reverse primer to subclone human LGI1 sequence with 3'UTR into pEGFP-N2 vector
human LGI1 (1-557)-His_6 3'UTR expression	hLGI1 -His-3'UTR -F	CATGTCATAGTTGACTTAAGCGCAGGA GGACATCATCACCATCACCATTGAGAC	Forward primer to subclone His_6 tag into pEGFP-N2 vector. It also contains the 5' sequence of human LGI1 and 3'UTR
	hLGI1 -His-3'UTR -R	GCAGCCACAGAATTTGGTGTCTCAATG GTGATGGTGATGATGTCCTCCTGCGCTT	Reverse primer to subclone His_6 tag into pEGFP-N2 vector. It also contains the 3' sequence of human LGI1 and 3'UTR
human LGI1 (37-557)-His_6 expression	XhoI-Igk -F	CTAGCTCGAGCCACCATGGAGACAGAC ACACTCCTGC	Forward primer to subclone human Igk-LGI1 sequence with His_6 tag into pEBMultii-neo vector
	LGI1-6His-NotI -R	ATTCGCGGCCGCTTAGTGATGGTGATGG TGGTGCTTTGCGCTTAAGTCAACTATGA	Reverse primer to subclone human Igk-LGI1 sequence with His_6 tag into pEBMultii-neo vector
human ADAM22 ECD (35-729)-FLAG expression	hADAM22 103-BamHI -F	GCTAGGATCCGAGCTAGAGAAGAGGAA GGAAAA	Forward primer to subclone human ADAM22 sequence into pAP tag5 vector
	hADAM22 2187-FLAG-BamHI -R	TAGCGGATCCCTACTTGTCGTCGTCATC CTTGTAGTCACCTCCGCCAGACAGAGT	Reverse primer to subclone human ADAM22 sequence into pAP tag5 vector containing C-terminal FLAG tag
human ADAM23 ECD (61-790)-FLAG expression	hADAM23 181-BglII -F	GCTAAGATCTCGGCCCCGCGCCTGGGG GGCTGC	Forward primer to subclone human ADAM23 sequence into pAP tag5 vector
	hADAM23 2370-FLAG-BglII -R	GCTAAGATCTCTACTTGTCGTCGTCATC CTTGTAGTCACCTCCGGCACTAGGACC	Reverse primer to subclone human ADAM23 sequence into pAP tag5 vector containing C-terminal FLAG tag
human LGI1 mutagenesis	hLGI1 F256A -F	ATGTAGTCATCGCTCAGCCTGCTACTGG AAAATGCATTTTCC	Forward primer to mutate human LGI1 Phe256 to Alanine
	hLGI1 F256A -R	GGAAAATGCATTTTCCAGTAGCAGGCT GAGCGATGACTACAT	Reverse primer to mutate human LGI1 Phe256 to Alanine
	hLGI1 V284A -F	CATTACAGGCACATCCACTGCAGTATGC AAGCCTATAGTCA	Forward primer to mutate human LGI1 Val284 to Alanine
	hLGI1 V284A -R	TGACTATAGGCTTGCATACTGCAGTGGA TGTGCCTGTAATG	Reverse primer to mutate human LGI1 Val284 to Alanine
	hLGI1 L302A -F	TCTATGTTATTGTGGCCCAGGCGTTTGG TGGCTCTCACATCTA	Forward primer to mutate human LGI1 Leu302 to Alanine
	hLGI1 L302A -R	TAGATGTGAGAGCCACCAAACGCCTGG GCCACAATAACATAGA	Reverse primer to mutate human LGI1 Leu302 to Alanine
	hLGI1 R330A -F	ATATTGAAATTCTCAAAATCGCAAAACC CAATGACATTGAAAC	Forward primer to mutate human LGI1 Arg330 to Alanine
	hLGI1 R330A -R	GTTTCAATGTCATTGGGTTTTGCGATTT TGAGAATTTCAATAT	Reverse primer to mutate human LGI1 Arg330 to Alanine
	hLGI1 K331A -F	TTGAAATTCTCAAAATCCGAGCACCCA ATGACATTGAAACAT	Forward primer to mutate human LGI1 Lys331 to Alanine
	hLGI1 K331A -R	ATGTTTCAATGTCATTGGGTGCTCGGAT TTTGAGAATTTCAA	Reverse primer to mutate human LGI1 Lys331 to Alanine
	hLGI1 K330A_K331A -F	ATATTGAAATTCTCAAAATCGCAGCACC CAATGACATTGAAACAT	Forward primer to mutate human LGI1 Arg330 to Alanine and Lys331 to Alanine
	hLGI1 K330A_K331A -R	ATGTTTCAATGTCATTGGGTGCTGCGAT TTTGAGAATTTCAATAT	Reverse primer to mutate human LGI1 Arg330 to Alanine and Lys331 to Alanine
	hLGI1 K353A -F	TTGTTGTTGCTGACAGTTCAGCAGCTG GTTTTACTACCATTT	Forward primer to mutate human LGI1 Lys353 to Alanine
	hLGI1 K353A -R	AAATGGTAGTAAAACCAGCTGCTGAAC TGTCAGCAACAACAA	Reverse primer to mutate human LGI1 Lys353 to Alanine
	hLGI1 R378A -F	AATCCTTACACGCGTGGTACGCGGACA CTGATGTGGAATATC	Forward primer to mutate human LGI1 Arg378 to Alanine
	hLGI1 R378A -R	GATATTCCACATCAGTGTCCGCGTACCA CGCGTGTAAGGATT	Reverse primer to mutate human LGI1 Arg378 to Alanine
	hLGI1 Y433A -F	TTCCTAACATGGAGGATGTGGCCGCAG TGAAGCACTTCTCAG	Forward primer to mutate human LGI1 Tyr433 to Alanine
	hLGI1 Y433A -R	CTGAGAAGTGCTTCACTGCGGCCACAT CCTCCATGTTAGGAA	Reverse primer to mutate human LGI1 Tyr433 to Alanine
	hLGI1 M477A -F	GGATGCCATCGCGAGGATCCGCGGTGT TCCAGCCTCTTCAAA	Forward primer to mutate human LGI1 Met477 to Alanine
	hLGI1 M477A -R	TTTGAAGAGGCTGGAACACCGCGGATC CTCGCGATGGCATCC	Reverse primer to mutate human LGI1 Met477 to Alanine
	hLGI1 E123K -F	ATCTAGAGTATTTATTCATAAAAAACAA CAACATCAAGTCAAT	Forward primer to mutate human LGI1 Glu123 to Lysine
	hLGI1 E123K -R	ATTGACTTGATGTTGTTGTTTTTTATGAA TAAATACTCTAGAT	Reverse primer to mutate human LGI1 Glu123 to Lysine
	hLGI1 R474Q -F	AGAGGATGCCATCGCGAGGATCCATGG TGTT	Forward primer to mutate human LGI1 Arg474 to Glutamine
	hLGI1 R474Q -R	AACACCATGGATCCTCGCGATGGCATCC TCT	Reverse primer to mutate human LGI1 Arg474 to Glutamine
	hLGI1 R407C -F	TCTAGTAGTTCCCAGTGTCCTGTAATTT ATC	Forward primer to mutate human LGI1 Arg407 to Cysteine
	hLGI1 R407C -R	GATAAATTACAGGACACTGGGAACTAC TAGA	Reverse primer to mutate human LGI1 Arg407 to Cysteine

Purpose	Primer Name	Primer Sequence (5' to 3')	Description
human ADAM22 mutagenesis	hADAM22 E359A -F	GAAAGGAGGAGGCGTGAATGCATTTGG GAAAACTGATTTAA	Forward primer to mutate human ADAM22 Glu359 to Alanine
	hADAM22 E359A -R	TTAAATCAGTTTTCCCAAATGCATTCAC GCCTCCTCCTTTC	Reverse primer to mutate human ADAM22 Glu359 to Alanine
	hADAM22 W398D -F	AATGTAAATGCGAGGACACGGACTCCG GGTGCATAATGGGAGA	Forward primer to mutate human ADAM22 Trp398 to Asparate
	hADAM22 W398D -R	TCTCCCATTATGCACCCGGAGTCCGTGT CCTCGCATTTACATT	Reverse primer to mutate human ADAM22 Trp398 to Asparate
	hADAM22 D405A -F	GTCCGGGTGCATAATGGGAGCCACTGG CTATTATCTTCCTA	Forward primer to mutate human ADAM22 Asp405 to Alanine
	hADAM22 D405A -R	TAGGAAGATAATAGCCAGTGGCTCCCAT TATGCACCCGGAC	Reverse primer to mutate human ADAM22 Asp405 to Alanine
	hADAM22 Y408A -F	GCATAATGGGAGACACTGGCGCTTATCT TCCTAAAAAGTTCA	Forward primer to mutate human ADAM22 Tyr408 to Alanine
	hADAM22 Y408A -R	TGAACTTTTTAGGAAGATAAGCGCCAG TGTCTCCCATTATGC	Reverse primer to mutate human ADAM22 Tyr408 to Alanine
	hADAM22 Y409A -F	TAATGGGAGACACTGGCTATGCTCTTCC TAAAAAGTTCACCC	Forward primer to mutate human ADAM22 Tyr409 to Alanine
	hADAM22 Y409A -R	GGGTGAACTTTTTAGGAAGAGCATAGC CAGTGTCTCCCATTA	Reverse primer to mutate human ADAM22 Tyr409 to Alanine
	hADAM22 Y408A_Y409A -F	GCATAATGGGAGACACTGGCGCTGCTC TTCCTAAAAAGTTCACCC	Forward primer to mutate human ADAM22 Tyr408 to Alanine and Tyr409 to Alanine
	hADAM22 Y408A_Y409A -R	GGGTGAACTTTTTAGGAAGAGCAGCGC CAGTGTCTCCCATTATGC	Reverse primer to mutate human ADAM22 Tyr408 to Alanine and Tyr409 to Alanine
Transgenic mouse genotyping	*Lgi1* WT -F	CAGATCCTTTGTGAGATCTGGTT	Forward primer for genotyping of mouse *Lgi*1 WT allele
	Lgi1 null -F	AGCGCATCGCCTTCTATCGCCTTC	Forward primer for genotyping of mouse *Lgi1* KO allele
	Lgi1 WT -R	AGAAGGCTTATCCGAATACATGCC	Reverse primer to for genotyping of mouse *Lgi1* WT allele
	Lgi1 FLAG-His_6 -F	GCTTGACCAGATTCATTGGCGACT	Forward primer for genotyping of FLAG-His_6 tagged-*Lgi1* transgene
	Lgi1 FLAG-His_6 -R	CTAATGGTGATGGTGATGATGACC	Reverse primer to for genotyping of FLAG-His_6 tagged-*Lgi1* transgene

Table 2. Summary of 28 ADLTE missense mutations on the LGI1 structure

Mutations	Nucleotide	Domain	Position	Structural/functional effects	Secretion	Reference
C42R	124T>C	LRR-NT	N-terminal Cys cap	Disruption of intramolecular disulfide bond with C48	Defective	8,9,29
C42G	124T>G	LRR-NT	N-terminal Cys cap	Disruption of intramolecular disulfide bond with C48	Defective	9,29,46
C46R	136T>C	LRR-NT	N-terminal Cys cap	Disruption of intramolecular disulfide bond with C55	Defective	9,29,47,48
C46F	137G>T	LRR-NT	N-terminal Cys cap	Disruption of intramolecular disulfide bond with C55	Not examined	30
I82T	245T>C	LRR 1	Structural core	Misfolding	Not examined	31
A110D	329C>A	LRR 2	Structural core	Misfolding	Defective	8,9,29
I122K	365T>A	LRR 3	Structural core	Misfolding	Defective	9,29,49
I122T	365T>C	LRR 3	Structural core	Misfolding	Defective	9,50
E123K	367G>A	LRR 3	Inter-LGI1 interface	Misfolding	Defective	9,29,39
R136W	406C>T	LRR 3	Structural core	Misfolding	Defective	9,29,50,51
S145R	435C>G	LRR 4	Structural core	Misfolding	Defective	9,29,52
L154P	461T>C	LRR 4	Structural core	Misfolding	Defective	9,29,53
C179R	535T>C	LRR-CT	C-terminal Cys cap	Disruption of intramolecular disulfide bond with C221	Defective	9,50
C200R	598T>C	LRR-CT	C-terminal Cys cap	Disruption of intramolecular disulfide bond with C177	Defective	9,29,54
L214P	641T>C	LRR-CT	Structural core	Misfolding	Not examined	55
F226C	677T>G	EPTP-Blade 7	Structural core (β-strand D)	Misfolding	Not examined	56
L232P	695T>C	EPTP-Blade 7	Structural core (β-strand D)	Misfolding	Defective	9,29,57
C286R	856T>C	EPTP-Blade 2	Structural core (β-strand A)	Disruption of intramolecular disulfide bond with C260	Not examined	32
I298T	893T>C	EPTP-Blade 2	Structural core (β-strand B)	Misfolding	Defective	8,9,29
F318C	953T>G	EPTP-Blade 2	Structural core (β-strand D)	Misfolding	Defective	9,29,58
L373S	1118T>C	EPTP-Blade 3	Structural core (β-strand D)	Misfolding	Not examined	32
T380A	No data	EPTP-Blade 4	Structural core (β-strand A)	Misfolding	Defective	9,33
E383A	1148A>C	EPTP-Blade 4	Structural core (β -strand A /Ca^{2+} coordination)	Misfolding	Defective	6,9,29
R407C	1219C>T	EPTP-Blade 4	Surface (Loop B-C)	Unaffected	Competent	9,35
V432E	1295T>A	EPTP-Blade 5	Structural core (Loop 4D-5A)	Misfolding	Defective	9,29,54
S473L	1418C>T	EPTP-Blade 5	Structural core (Loop 5D-6A)	Disruption of the binding to ADAM22	Competent	9,29,36,46
R474Q	1421G>A	EPTP-Blade 6	Inter-LGI1 interface (Loop 5D-6A)	Disruption of LGI1 dimer formation	Competent	9,36
G493R	1477G>A	EPTP-Blade 6	Structural core (Loop B-C)	Misfolding	Defective	9,59

Table 3. Summary of LGI1 variants mapped on the LGI1 structure

Alterations	Nucleotide	Domain
V45M	133G>A	LRR-NT
D51H	151G>C	LRR-NT
D51V	152A>T	LRR-NT
D51E	153T>A	LRR-NT
N52T	155A>C	LRR-NT
A53V	158C>T	LRR-NT
S60C	179C>G	LRR-NT
R63C	187C>T	LRR-NT
T64I	191C>T	LRR-NT
D68E	204T>A	LRR-NT
V69I	205G>A	LRR-NT
I82L	244A>C	LRR 1
S83L	248C>T	LRR 1
T90M	269C>T	LRR 1
S92L	275C>T	LRR1
N101D	301A>G	LRR 2
D104N	310G>A	LRR 2
D108G	323A>G	LRR 2
A110V	329C>T	LRR 2
P115L	344C>T	LRR 2
N124S	371A>G	LRR 3
N125K	375C>A	LRR 3
R132T	395G>C	LRR 3
H133R	398A>G	LRR 3
R136Q	407G>A	LRR 3
G161C	481G>T	LRR 4
T166A	496A>G	LRR 4
D169N	505G>A	LRR 5
N176T	527A>C	LRR-CT
L188F	562C>T	LRR-CT
H190Y	568C>T	LRR-CT
N192S	575A>G	LRR-CT
V195I	583G>A	LRR-CT
E201A	602A>C	LRR-CT
Y206C	617A>G	LRR-CT
R209C	625C>T	LRR-CT
R209H	626G>A	LRR-CT
K210N	630A>T	LRR-CT
N212D	634A>G	LRR-CT
S213C	637A>T	LRR-CT
S213R	639T>A	LRR-CT
L214F	640C>T	LRR-CT
S216L	647C>T	LRR-CT
D220N	658G>A	LRR-CT
D220E	660T>G	LRR-CT
I223V	667A>G	Linker
A227V	680C>T	EPTP-Blade 7
I239T	716T>C	EPTP-Blade 1
T241N	722C>A	EPTP-Blade 1
N246K	738T>A	EPTP-Blade 1
A253T	757G>A	EPTP-Blade 1
I261L	781A>C	EPTP-Blade 1
F262L	786C>G	EPTP-Blade 1
D266N	796G>A	EPTP-Blade 1
V268M	802G>A	EPTP-Blade 1
K270N	810G>T	EPTP-Blade 1
T271I	812C>T	EPTP-Blade 1
T271N	812C>A	EPTP-Blade 1
R273W	817C>T	EPTP-Blade 1
N277D	829A>G	EPTP-Blade 1
T279A	835A>G	EPTP-Blade 1
S282P	844T>C	EPTP-Blade 1-2
I289L	865A>C	EPTP-Blade 2
I291V	871A>G	EPTP-Blade 2
Y296C	887A>G	EPTP-Blade 2
V299A	896T>C	EPTP-Blade 2
F303L	907T>C	EPTP-Blade 2
G305D	914G>A	EPTP-Blade 2
I308V	922A>G	EPTP-Blade 2
R311Q	932G>A	EPTP-Blade 2
S313G	937A>G	EPTP-Blade 2
S313R	939T>A	EPTP-Blade 2
N316T	947A>C	EPTP-Blade 2
N316S	947A>G	EPTP-Blade 2
K328R	983A>G	EPTP-Blade 3
R330Q	989G>A	EPTP-Blade 3
N333S	998A>G	EPTP-Blade 3
K339N	1017G>C	EPTP-Blade 3
I340T	1019T>C	EPTP-Blade 3
N342T	1025A>C	EPTP-Blade 3
V348F	1042G>T	EPTP-Blade 3
A354S	1060G>T	EPTP-Blade 3
F356L	1066T>C	EPTP-Blade 3
I359L	1075A>C	EPTP-Blade 3
I359V	1075A>G	EPTP-Blade 3
I359T	1076T>C	EPTP-Blade 3
K361Q	1081A>C	EPTP-Blade 3
K361N	1083A>C	EPTP-Blade 3
S369F	1106C>T	EPTP-Blade 3
H370R	1109A>G	EPTP-Blade 3
A375T	1123G>A	EPTP-Blade 3-4
A375P	1123G>C	EPTP-Blade 3-4
A375V	1124C>T	EPTP-Blade 3-4
A375G	1124C>G	EPTP-Blade 3-4
Y377H	1129T>C	EPTP-Blade 3-4
T390I	1169C>T	EPTP-Blade 4
Q392H	1176G>C	EPTP-Blade 4
L394F	1180C>T	EPTP-Blade 4
P397T	1189C>A	EPTP-Blade 4
S402C	1205C>G	EPTP-Blade 4
R407C	1219C>T	EPTP-Blade 4
R407H	1220G>A	EPTP-Blade 4
N414D	1240A>G	EPTP-Blade 4
A416T	1246G>A	EPTP-Blade 4
N422K	1266C>G	EPTP-Blade 4-5
M429V	1285A>G	EPTP-Blade 4-5
D431V	1292A>T	EPTP-Blade 4-5
A434T	1300G>A	EPTP-Blade 5
A434S	1300G>T	EPTP-Blade 5
S439L	1316C>T	EPTP-Blade 5
V440M	1318G>A	EPTP-Blade 5
V440A	1319T>C	EPTP-Blade 5
G442E	1325G>A	EPTP-Blade 5
D443E	1329C>A	EPTP-Blade 5
V444M	1330G>A	EPTP-Blade 5
V444L	1330G>T	EPTP-Blade 5
V444E	1331T>A	EPTP-Blade 5
I446L	1336A>C	EPTP-Blade 5
I446V	1336A>G	EPTP-Blade 5
K456R	1367A>G	EPTP-Blade 5
K456N	1368A>C	EPTP-Blade 5
M458L	1372A>C	EPTP-Blade 5
S463F	1388C>T	EPTP-Blade 5
S464L	1391C>T	EPTP-Blade 5
Q466R	1397A>G	EPTP-Blade 5
M471V	1411A>G	EPTP-Blade 5
M477V	1429A>G	EPTP-Blade 5-6
Q483R	1448A>G	EPTP-Blade 6
Y487H	1459T>C	EPTP-Blade 6
I491V	1471A>G	EPTP-Blade 6
D505N	1513G>A	EPTP-Blade 6
A506P	1516G>C	EPTP-Blade 6
A506S	1516G>T	EPTP-Blade 6
A506E	1517C>A	EPTP-Blade 6
A509T	1525G>A	EPTP-Blade 6
V519A	1556T>C	EPTP-Blade 6-7
V528L	1582G>T	EPTP-Blade 7
S529F	1586C>T	EPTP-Blade 7
I530T	1589T>C	EPTP-Blade 7
N531K	1593T>A	EPTP-Blade 7
R533C	1597C>T	EPTP-Blade 7
R533H	1598G>A	EPTP-Blade 7
V551F	1651G>T	EPTP-Blade 7
V551A	1652T>C	EPTP-Blade 7

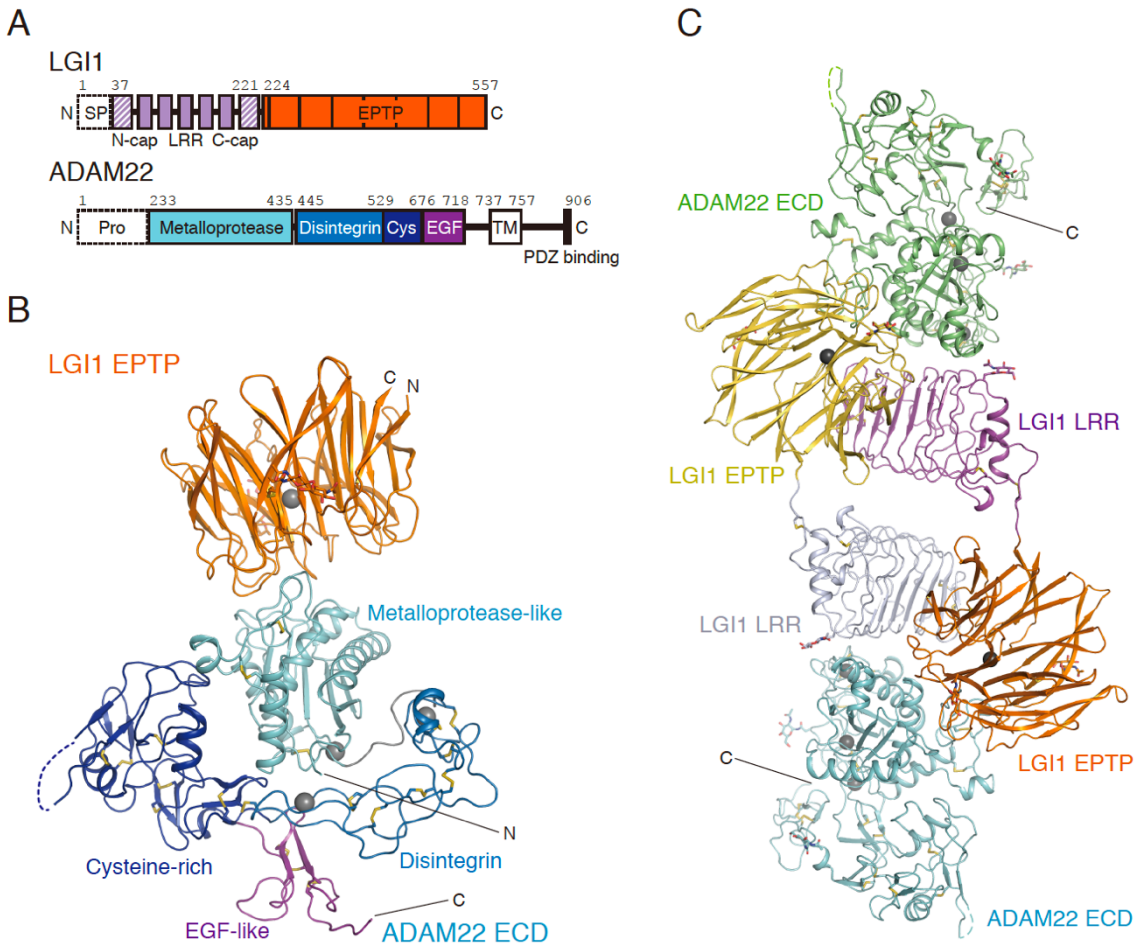

Figure 1. Structure of LGI1–ADAM22 ECD complex

(A) Domain organizations of LGI1 and ADAM22. LGI1 consists of the LRR (purple) and EPTP (orange) domains. The N-terminal secretion signal peptide (SP, enclosed by dotted lines) is removed in the secreted LGI1. The shaded purple boxes represent the N- and C-terminal caps, whereas the filled purple boxes represent the LRRs. The orange boxes represent the blades of the β-propeller. The premature form of ADAM22 contains the N-terminal prosequence (enclosed by dotted lines). The mature ADAM22 consists of the metalloprotease-like (cyan), disintegrin (light blue), cysteine-rich (dark blue), EGF-like (purple), transmembrane (white) and cytoplasmic domains. The major ADAM22 isoform has a PDZ-binding motif in the C-terminal region of the cytoplasmic domain.

(B) Overall structure of LGI1 EPTP–ADAM22 ECD complex. The bound calcium ions are shown as grey spheres. The N-linked sugar chains and disulfide bonds are shown as sticks. The coloring scheme is the same as that in (A).

(C) Overall structure of the 2:2 LGI1–ADAM22 complex. LGI1 LRR, LGI1 EPTP and ADAM22 ECD in one LGI1–ADAM22 pair are colored in magenta, orange and cyan, respectively, whereas those in the other pair are colored in grey, light yellow and light green, respectively. The length along the longest axis of the 2:2 LGI1–ADAM22 complex is about 190 Å.

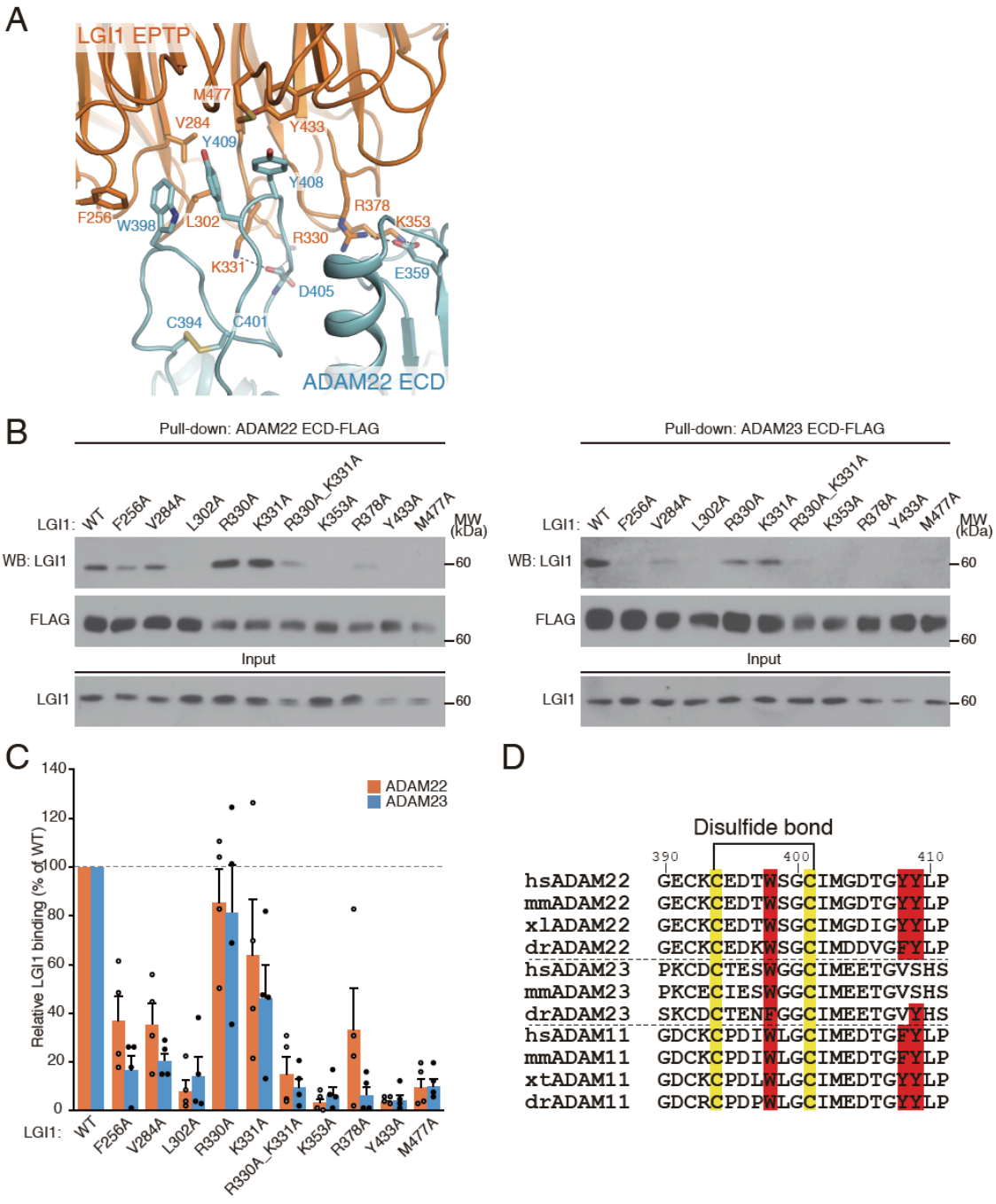
A
LGI1 EPTP
M477
V284
Y433
Y409
Y408
R378
F256
W398
L302
K353
R330
K331
E359
D405
C394
C401
ADAM22 ECD
B
Pull-down: ADAM22 ECD-FLAG
Pull-down: ADAM23 ECD-FLAG
LGI1: WT F256A V284A L302A R330A K331A R330A_K331A K353A R378A Y433A M477A
MW (kDa)
WB: LGI1
FLAG
Input
LGI1
60
C
ADAM22
ADAM23
Relative LGI1 binding (% of WT)
140
120
100
80
60
40
20
0
LGI1: WT F256A V284A L302A R330A K331A R330A_K331A K353A R378A Y433A M477A
D
Disulfide bond
390
400
410
hsADAM22 GECKCEDTWSGCIMGDTGYYLP
mmADAM22 GECKCEDTWSGCIMGDTGYYLP
xlADAM22 GECKCEDTWSGCIMGDIGYYLP
drADAM22 GECKCEDKWSGCIMDDVGFYLP
hsADAM23 PKCDCTESWGGCIMEETGVSHS
mmADAM23 PKCECIESWGGCIMEETGVSHS
drADAM23 SKCDCTENFGGCIMEETGVYHS
hsADAM11 GDCKCPDIWLGCIMEDTGFYLP
mmADAM11 GDCKCPDIWLGCIMEDTGFYLP
xtADAM11 GDCKCPDLWLGCIMEDTGYYLP
drADAM11 GDCRCPDPWLGCIMEDTGYYLP

Figure 2. Site-directed mutational analysis of the interaction between LGI1 and ADAM22 or ADAM23

(A) Close-up view of the interface between LGI1 EPTP and ADAM22 ECD. The residues involved in their binding and a disulfide bond between Cys394 and Cys401 of ADAM22 are shown as sticks. Hydrogen bonds are shown as dotted lines. The coloring scheme is the same as that in Fig. 1B.

(B, C) Pull-down assay between LGI1 mutants and ADAM22 or ADAM23 ECD. Indicated LGI1 mutants and ADAM22 or ADAM23 ECD-FLAG secreted from HEK293T cells were mixed and pulled-down with anti-FLAG antibody agarose. Shown are Western blots of the (co-)purified (upper two panels) and input (bottom) samples with indicated antibodies (B). Quantification of the amounts of the co-purified LGI1 with ADAM22 ECD-FLAG (orange) or with ADAM23 ECD-FLAG (light blue) is shown in the graph (C). n = 4 independent experiments. Results are shown as mean ± s.e.

(D) Amino-acid sequence alignment of ADAM22, ADAM23 and ADAM11 from representative vertebrates (hs, Homo sapiens; mm; Mus musculus; xl, Xenopus laevis; xt, Xenopus tropicalis; dr, Danio rerio), generated by ClustalW2.

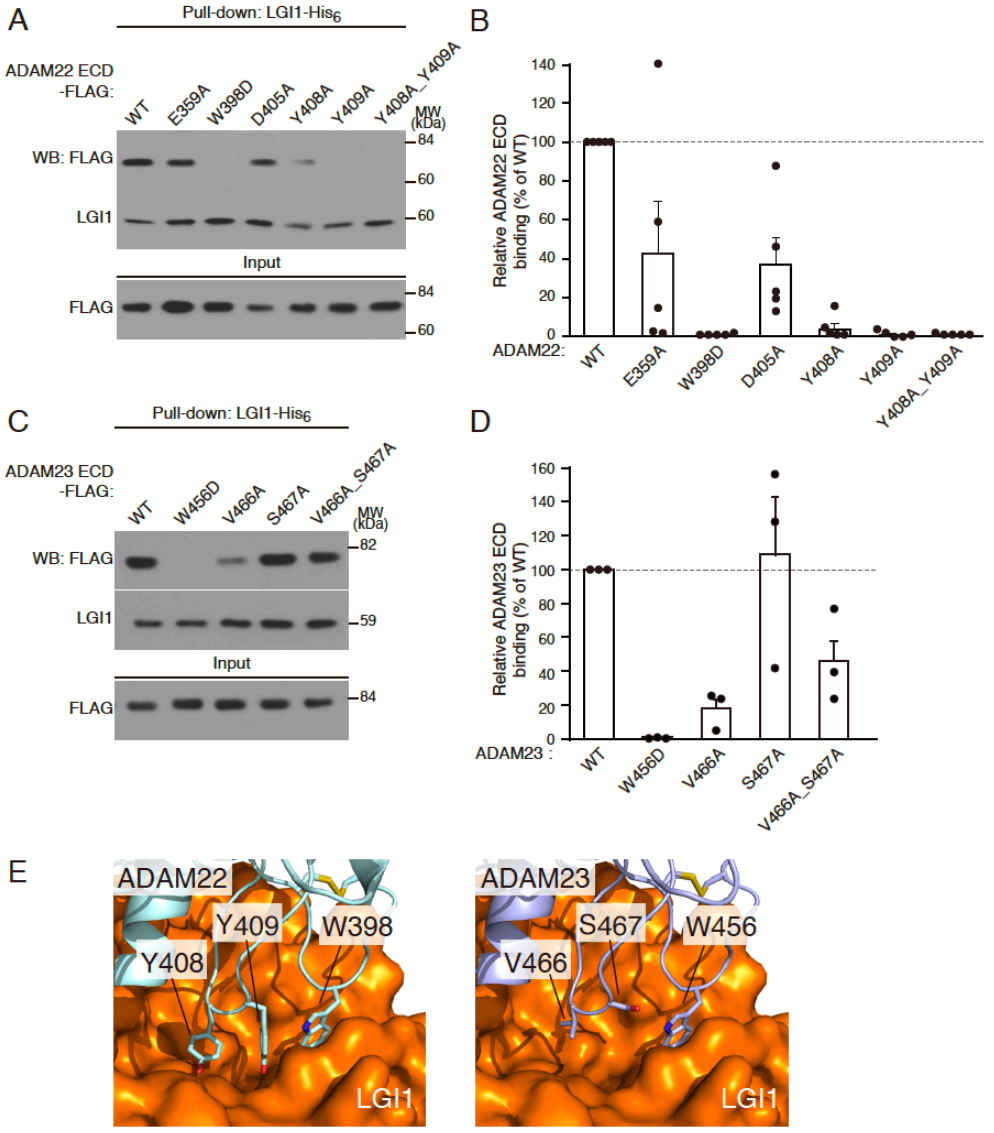

Figure 3.

Conservation of the essential hydrophobic interaction between LGI1–ADAM22 and LGI1–ADAM23

(A-D) Pull-down assay between LGI1-His_6 and ADAM22 or ADAM23 ECD-FLAG mutants. LGI1-His_6 and the indicated ADAM22 or ADAM23 mutant proteins secreted from HEK293T cells were mixed and pulled-down with Ni-NTA agarose. Shown are Western blots (WB) of the (co-)purified (upper two panels) and input (bottom) samples with indicated antibodies (A, C). Quantification of the amounts of the co-purified ADAM22 or ADAM23 ECD mutant proteins with LGI1 is shown in the graph (B, D). n = 5 and 3 independent experiments for (A, B) and (C, D), respectively. Results are shown as mean ± s.e.

(E) Close-up view of the hydrophobic interface of the LGI1 EPTP–ADAM22 ECD (left) and LGI1 EPTP–ADAM23 ECD (right). The structure of ADAM23 was modeled by SWISS-MODEL using the ADAM22 structure in LGI1–ADAM22 complex (PDB 5Y31) as a template. Trp398, Tyr408 and Tyr409 of ADAM22 and Trp456, Val466 and Ser467 of ADAM23 are shown as sticks. The binding sites of LGI1 are shown as surfaces.

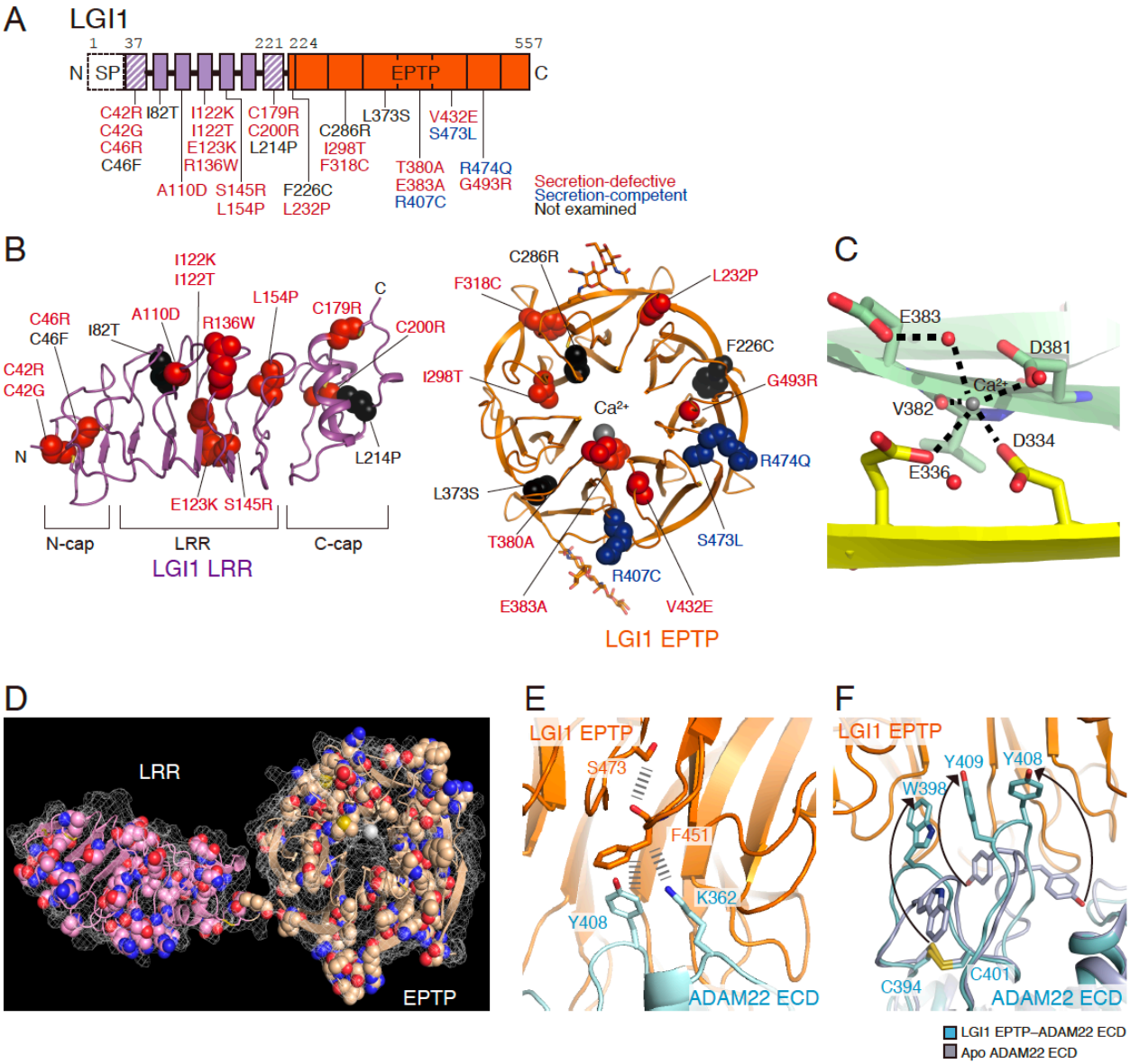
A
LGI1
1
37
221
224
557
N
SP
EPTP
C
C42R
C42G
C46R
C46F
I82T
A110D
I122K
I122T
E123K
R136W
S145R
L154P
C179R
C200R
L214P
F226C
L232P
C286R
I298T
F318C
L373S
T380A
E383A
R407C
V432E
S473L
R474Q
G493R
Secretion-defective
Secretion-competent
Not examined
B
I122K
I122T
C46R
C46F
I82T
A110D
R136W
L154P
C179R
C
C200R
C42R
C42G
N
L214P
E123K
S145R
N-cap
LRR
C-cap
LGI1 LRR
C286R
F318C
L232P
F226C
I298T
G493R
Ca2+
R474Q
L373S
S473L
T380A
R407C
E383A
V432E
LGI1 EPTP
C
E383
D381
Ca2+
V382
D334
E336
D
LRR
EPTP
E
LGI1 EPTP
S473
F451
K362
Y408
ADAM22 ECD
F
LGI1 EPTP
Y409
Y408
W398
C401
C394
ADAM22 ECD
LGI1 EPTP–ADAM22 ECD
Apo ADAM22 ECD

Figure 4. Missense ADLTE mutations in LGI1

(A) Schematic representation of 28 missense ADLTE mutations in LGI1 (red, secretion-defective; blue, secretion-competent; black, not examined). The drawing scheme of the domain organization of LGI1 is the same as that in Fig. 1A.

(B) Mapping of 28 missense ADLTE mutations in LGI1 LRR and EPTP on the LGI1 structure. The amino-acid residues in the mutation sites are shown as spheres. The coloring scheme of the mutation sites is the same as that in (A).

(C) Ca^{2+}-binding site in the LGI1 EPTP β-propeller. Ca^{2+} and water molecules are shown as grey and red spheres, respectively. Hydrogen bonds are shown as dotted lines.

(D) Mapping of 144 amino-acid the alterations reported in gnomAD on the LGI1 structure. The amino-acid residues at which alterations occur are shown as spheres with gray for Ca^{2+}, red for oxygen atoms and blue for nitrogen atoms. The surface of the protein is shown as mesh. The variants are listed in Table 3.

(E) Close-up view of the area around Ser473 of LGI1 at the interface between LGI1 EPTP and ADAM22 ECD. Dotted lines represent putative steric clashes occurring in $LGI1^{S473L}$ and between $LGI1^{S473L}$ and ADAM22 ECD.

(F) Conformational change in Trp398, Tyr408 and Tyr409 of ADAM22 upon binding to LGI1 EPTP. The apo-ADAM22 structure (light purple, PDB 3G5C) is superposed onto the LGI1 EPTP–ADAM22 ECD structure (cyan).

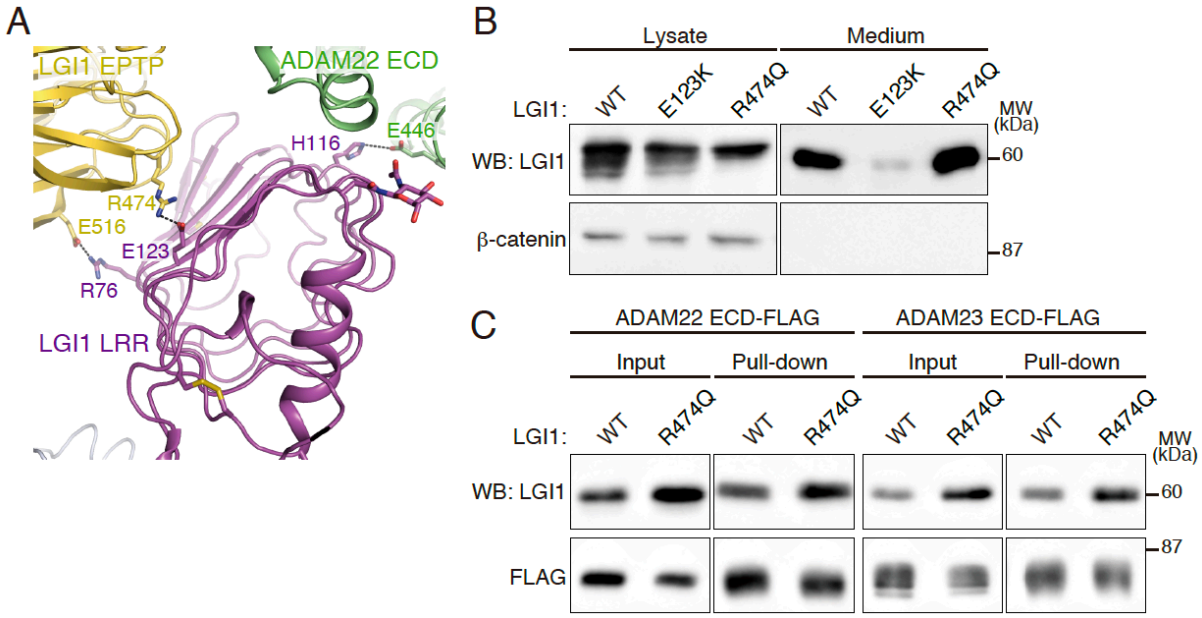

Figure 5. Characterization of ADLTE mutations in LGI1-LGI1 interface *in vitro*

(A) Close-up view of the LGI1 LRR–LGI1 EPTP and LGI1 LRR–ADAM22 ECD interfaces in the 2:2 LGI1–ADAM22 complex. The residues likely involved in these interfaces are shown as sticks. The coloring scheme is the same as that in Fig. 1C.

(B) Secretion of $LGI1^{E123K}$ and $LGI1^{R474Q}$ proteins from transfected HEK293T cells. Shown are Western blots of the cell lysates and the conditioned medium with indicated antibodies.

(C) Pull-down assay between $LGI1^{WT}$ or $LGI1^{R474Q}$ and ADAM22 or ADAM23 ECD-FLAG. Shown are Western blots of the (co-)purified (pulled-down with FLAG antibody agarose) and input samples with indicated antibodies.

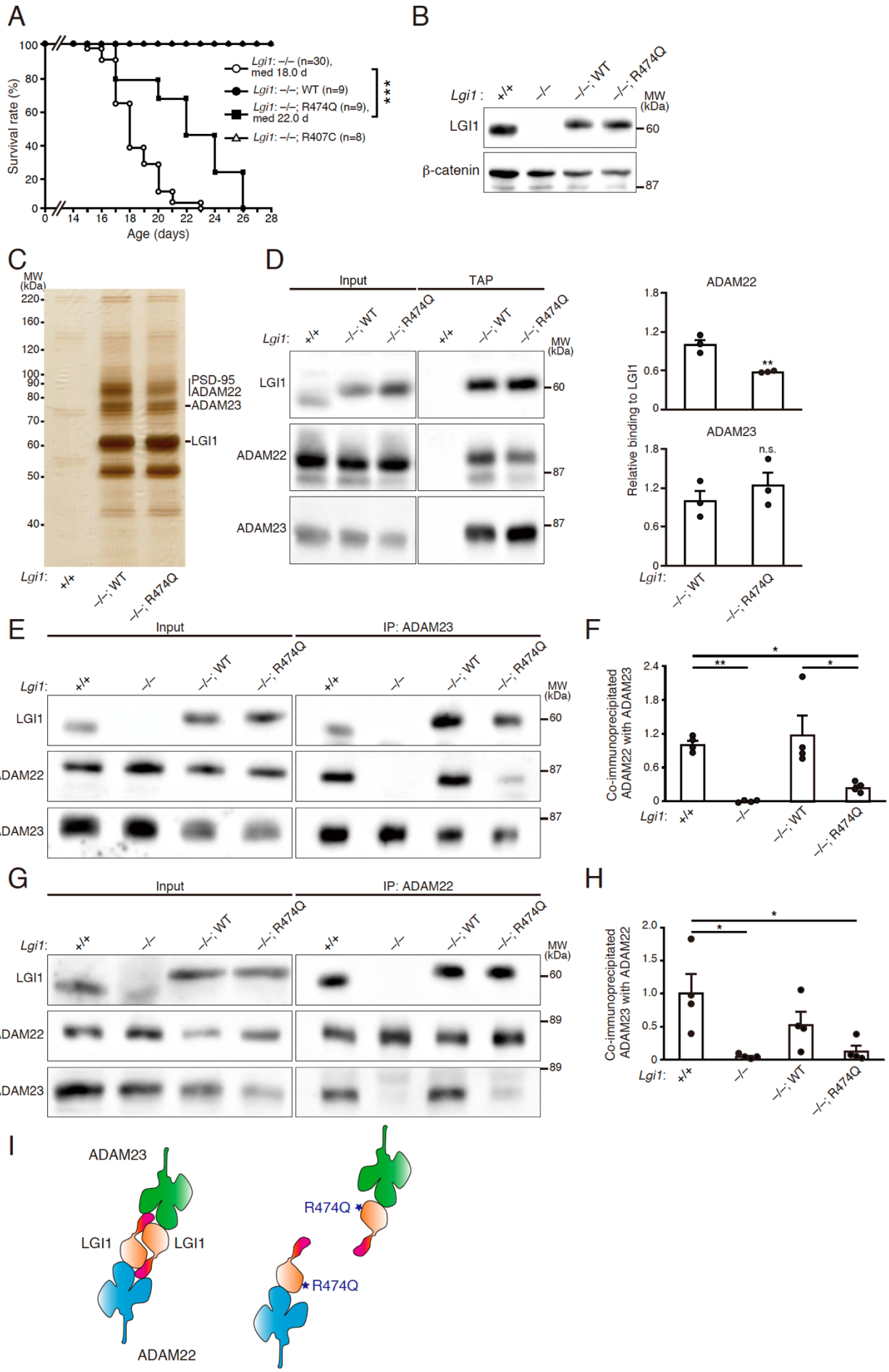
A
Survival rate (%)
Age (days)
Lgi1: –/– (n=30), med 18.0 d
Lgi1: –/–; WT (n=9)
Lgi1: –/–; R474Q (n=9), med 22.0 d
Lgi1: –/–; R407C (n=8)
***
B
Lgi1 :
MW (kDa)
LGI1
β-catenin
C
PSD-95
ADAM22
ADAM23
LGI1
D
Input
TAP
ADAM22
ADAM23
Relative binding to LGI1
n.s.
E
Input
IP: ADAM23
F
Co-immunoprecipitated ADAM22 with ADAM23
G
Input
IP: ADAM22
H
Co-immunoprecipitated ADAM23 with ADAM22
I
ADAM23
LGI1
LGI1
ADAM22
R474Q
R474Q

Figure 6. Pathogenic mechanism of a secretion-competent ADLTE mutation, LGI1^{R474Q}

(A) Kaplan–Meier survival plots of mice with secretion-competent ADLTE mutations, LGI1^{R474Q} and LGI1^{R407C}. ***P < 0.001, log-rank test.

(B) Loss of LGI1 in *Lgi1*$^{-/-}$ mice and reexpression of LGI1 in *Lgi1*$^{-/-;WT}$ mice and *Lgi1*$^{-/-;R474Q}$ mice were confirmed by Western blots of brain lysates with indicated antibodies.

(C, D) Tandem-affinity purification (TAP) of LGI1^{WT} and LGI1^{R474Q} tagged with FLAG and His_6 from the indicated mouse brain extracts. Shown are the silver staining of TAP eluates (C) and Western blots of input (left) and TAP eluates (right) with indicated antibodies (D). Quantification of the amount of co-purified ADAM22 and ADAM23 with tagged LGI1 is shown in the right graph (D). Known co-purified proteins were indicated (C). **P < 0.01; n.s., not significant; n = 3 independent experiments (D). Two-tailed Student's t test was used.

(E, F) Immunoprecipitation (IP) of ADAM23 from the indicated mouse brain extracts. Shown are Western blots of input (left) and IP (right) samples with indicated antibodies (E). Quantification of the amount of ADAM22 co-immunoprecipitated with ADAM23 is shown in the graph (F).

(G, H) IP of ADAM22 from the indicated mouse brain extracts. **P < 0.01; *P < 0.05; n = 4 independent experiments. One-way ANOVA followed by post hoc Tukey's test was used (F, H). Results are shown as mean ± s.e.

(I) Model of tripartite complex comprising ADAM22–LGI1–ADAM23 at 1:2:1 stoichiometry. Two heterodimers, LGI1–ADAM22 and LGI1–ADAM23, are arranged in the LGI1-mediated head-to-head configuration to form the tetrameric complex (left). The R474Q mutation (asterisk) in LGI1 disrupts the LGI1–LGI1 interaction (right).

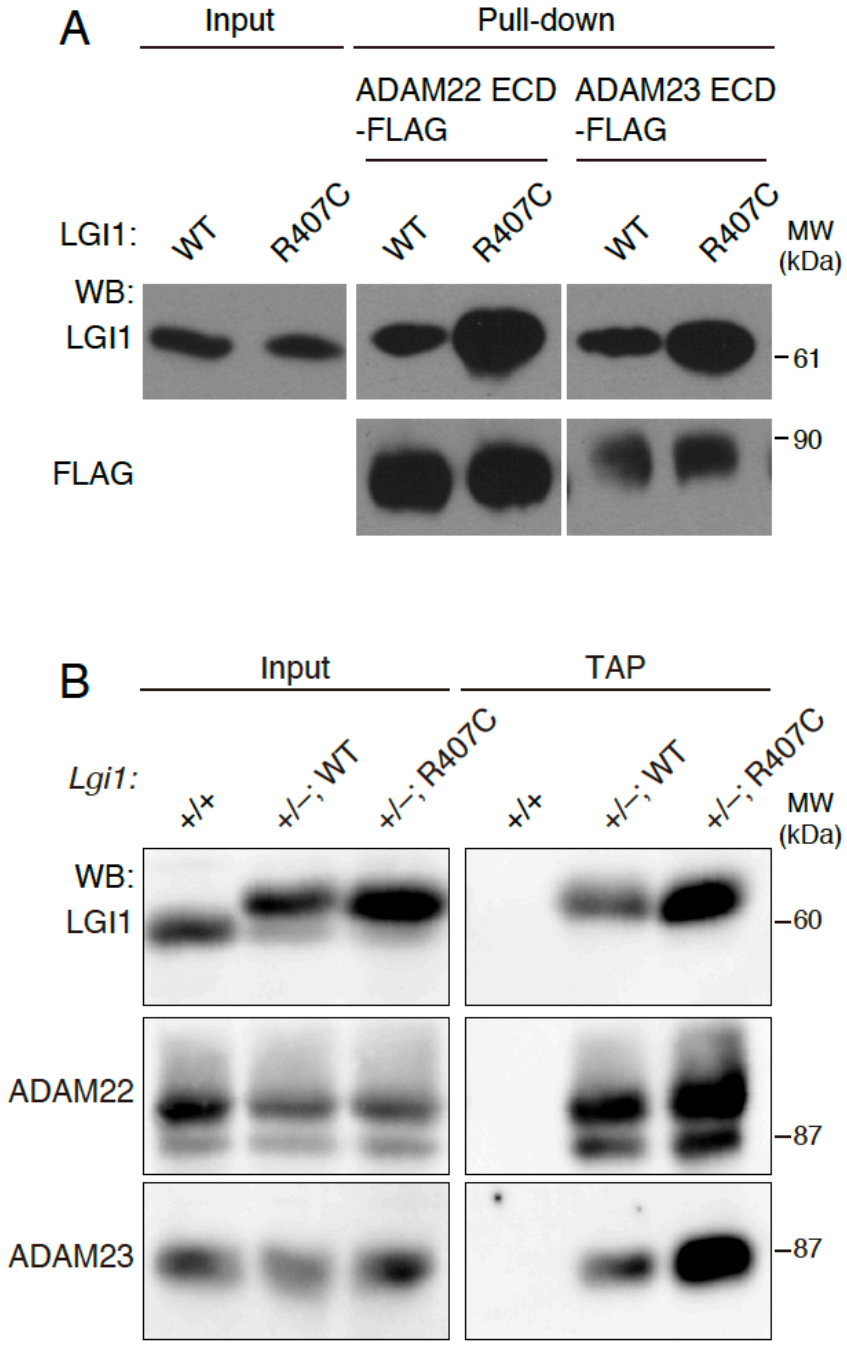

Figure 7. Non-pathogenic mutation of LGI1, LGI1^{R407C}

(A) Pull-down assay between LGI1^{WT} or LGI1^{R407C} and ADAM22 or ADAM23 ECD-FLAG. LGI1^{WT} or LGI1^{R407C} and ADAM ECD-FLAG secreted from HEK293T cells were mixed and pulled-down with FLAG antibody agarose. Shown are Western blots of input (left) and (co-)purified (right two panels) samples with indicated antibodies.

(B) TAP of LGI1^{WT} and LGI1^{R407C} tagged with FLAG and His_6 from the mouse brain, showing that ADAM22 and ADAM23 were enriched with purified LGI1^{WT} and LGI1^{R407C} similarly. Shown are Western blots of input (left) and TAP eluates (right) with indicated antibodies.

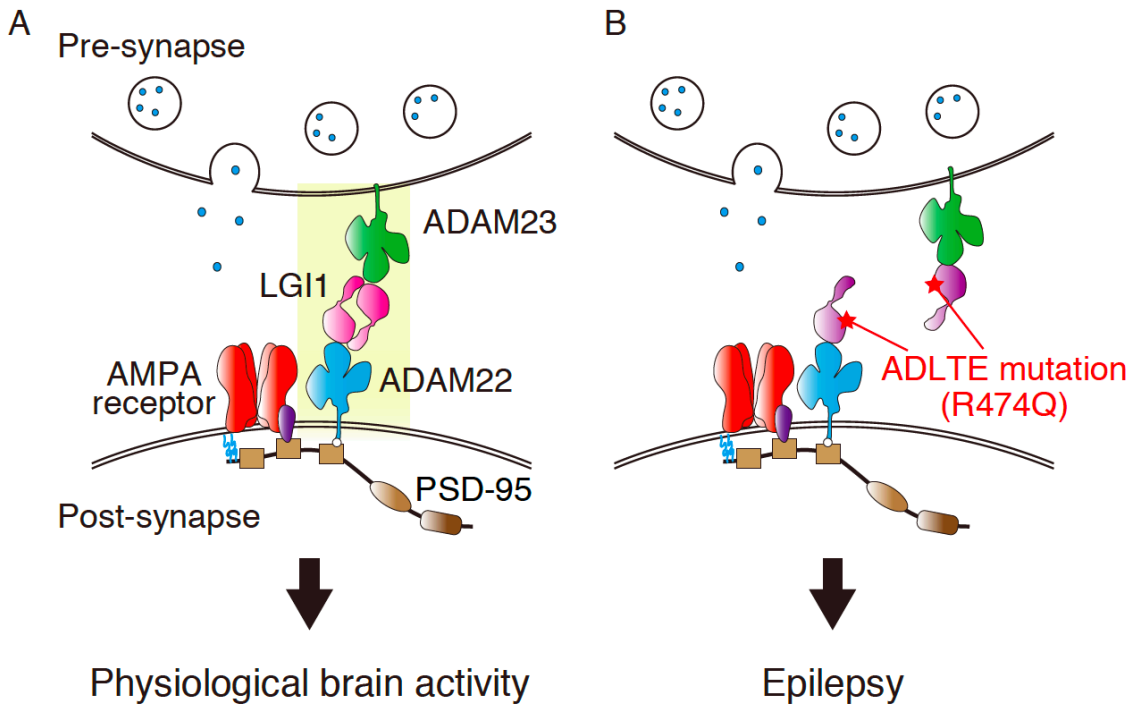

Figure 8. Model of the *trans*-synaptic linkage mediated by LGI1–ADAM22/ADAM23 higher-order assembly

(A) The higher-order assembly of LGI1–ADAM22/23 mediates the *trans*-synaptic linkage and is required for the physiological brain activity.

(B) The disruption of the *trans*-synaptic linkage including the defects in LGI1–LGI1 interaction by ADLTE mutations causes epilepsy.